Follicular mural granulosa cells stockpile glycogen to fuel corpus luteum pre-vascularization

Jianning Liao[1†], Qinghua Liu[1†], Cong Liu[2†], Guiqiong Liu[1†], Xiang Li[1†], Xiaodong Wang[1], Yaqin Wang[2], Ruiyan Liu[1], Hao Wu[3], Hongru Shi[1], Yongheng Zhao[1], Wenkai Ke[1], Zaohong Ran[1], Zian Wu[1], Bowen Tan[1], Chaoli Wang[4], Xunping Jiang[1], Quanfeng Wang[5], Qingzhen Xie[2*], Guoshi Liu[3*], Changjiu He[1*]

[1] Key Laboratory of Agricultural Animal Genetics, Breeding and Reproduction of Ministry of Education, College of Animal Sciences and Technology, Huazhong Agricultural University, Wuhan 430070, PR China;

[2] Centre for Reproductive Medicine, Renmin Hospital of Wuhan University, Wuhan 430000, China.

[3] Key Laboratory of Animal Genetics and Breeding of the Ministry of Agriculture, College of Animal Science and Technology, China Agricultural University, Beijing, China

[4] Xinjiang Western Animal Husbandry Co., Ltd, Shihezi, China.

[5] Xinjiang Jinken aoqun agriculture and animal husbandry technology Co., Ltd, Hetian, China.

[†] These authors contributed equally to this work.

***Corresponding Author**:
Changjiu He,
Orcid ID: 0000-0002-0350-9799;
Email: chungjoe@mail.hzau.edu.cn; Huazhong Agricultural University, Wuhan 430070, China.
Guoshi Liu
Orcid ID: 0000-0002-5688-3645;
Email: gshliu@cau.edu.cn; China Agricultural University, Beijing 100193, China
Qingzhen Xie,
Orcid ID: 0000-0002-4628-4278;
Email: rm001138@whu.edu.cn; Renmin Hospital of Wuhan University, Wuhan 430000, China.

Short title: fGCs store glycogen for corpus luteum

ABSTRACT

The differentiation of follicular mural granulosa cells (fGCs) into luteal cells involves a rapid progesterone synthesis surge and the vascular network development. However, progesterone elevation occurs before vascularization, leaving luteinizing fGCs temporarily devoid of blood supply. The mechanism of how fGCs fuel increased progesterone synthesis during this avascular phase remains unclear. Our research, utilizing integrative single-cell/spatial transcriptomics analysis and in vivo/ex vivo experiments, revealed that upon receiving the ovulatory/luteinization signal, fGCs transition to a low-energy state, reducing metabolic activity and storing glucose as glycogen. This process is governed by the LH (hCG)-Ras/Raf/Mek/Erk-RUNX1-Insulin signaling cascade. By mobilizing glycogen storage pre-vascularization, fGCs are fueled for enhanced progesterone synthesis. Supplementing glucose enhanced glycogen storage, leading to heightened progesterone secretion in corpora lutea. Implementing this technique, we enhanced luteal function in mice, sheep, and humans, resulting in increased litter rate in mice and improved pregnancy rates in sheep. Our study introduces the innovative concept of "fGC energy storage" and establishes the "Luteal Function Enhancement Technique", contributing to the theoretical basis of reproductive physiology and displaying substantial clinical implications.

Keywords: ovulation, glycogen, granulosa cell, corpus luteum, follicle, luteinization

INTRODUCTION

Ovulation plays a crucial role in successful reproduction, encompassing the release of the cumulus-oocyte complex and luteinization of fGCs (including theca cells).[1, 2] The resulting corpus luteum, though transient, is essential for reproductive health.[3] It drives the estrous cycle through cyclical formation and regression, while also being vital for maintaining pregnancy.[4, 5] Primarily responsible for progesterone secretion, the corpus luteum is among the most metabolically active tissues in the body.[6] To meet the demand for large-scale synthesis and transport of progesterone, the corpus luteum is highly vascularized to ensure sufficient blood supply to all luteal cells.[7-9]

Insufficient luteal function is a common gynecological disorder characterized by inadequate progesterone secretion, leading to menstrual irregularities, fertility issues, and recurrent miscarriages. [10-12] Statistics indicate a considerable proportion of infertility cases in women are attributed to insufficient luteal function, underscoring its significant impact on reproductive health.[13] As a result, exploring the mechanisms of ovulation/luteinization remains a key focus of reproductive research.

Ovulation/luteinization are initiated by the pre-ovulatory surge of luteinizing hormone (LH) or human chorionic gonadotropin (hCG). fGCs primarily function to receive and transmit the ovulation/luteinization signal.[14] Upon signal reception, fGCs cease proliferation, leading to cell cycle arrest in the G0/G1 phase.[15, 16] This is followed by stiffening of the fGC-layer, enhancing the physical connection between fGCs and the extracellular matrix to prevent their escape from the ruptured follicle.[17] Subsequently, a shift in steroidogenic gene expression patterns occurs within fGCs, with genes responsible for estrogen synthesis being silenced and those involved in progesterone synthesis experiencing a sharp increase in expression.[18, 19] The luteinizing fGCs then extend pseudopodia and migrate inward to fill the remnant follicular antrum following the release of the cumulus-oocyte complex.[20, 21] Endothelial cells subsequently invade the remnant antrum, forming the vascular network.[22] Various signaling cascades, including cAMP/PKA, PLC/PKC, PI3K/Akt/Sgk/Foxo, Ras/Raf/Mek/Erk, and PRL/Jak/Stat, have been implicated in regulating luteinization.[23-27] Key transcription factors such as CEBPα/β, Egr-1, Nur-77, Nr5a1, and Runx1/2 have also been identified as critical regulators of luteal functional gene expression.[28-32]

Although entailing intricate cytological changes and signal mobilization, the formation of corpus luteum can be simplified into two fundamental processes. Firstly, fGCs undergo differentiation into luteinized fGCs, known as luteal cells, characterized by a significant increase in progesterone synthesis. In mice, for example, the injection of hCG triggers a rapid surge in progesterone synthesis, escalating from several nanograms to hundreds of nanograms within just 9 hours. This surge necessitates that

the luteinized fGCs adjust their metabolic profile to generate energy levels well above the norm. Secondly, the development of a vascular network ensues; a mature corpus luteum features a well-established internal vascular network, ensuring each luteal cell is closely associated with capillaries, facilitating sufficient energy and material support for robust hormone synthesis.[22] Interestingly, the luteinization of fGCs precedes the formation of the vascular network significantly, implying that the developing corpus luteum inevitably undergoes a period devoid of blood vessels. This presents a longstanding puzzle: how do luteinized fGCs ensure an adequate supply of energy and materials to sustain their intense hormonal activities during the avascular phase?

Our study aims to propose a theoretical model to elucidate this question. Through transcriptomic analysis and gene editing techniques, we identified a highly conserved reproductive event termed “fGC energy storage” following ovulatory/luteinization stimulation. Upon receiving the stimulus, fGCs transition to an energy-saving mode, reducing metabolic intensity, limiting carbohydrate breakdown, and lowering ATP production. Meanwhile, fGCs increase glucose uptake and store it as glycogen in the cytoplasm. This stored glycogen is subsequently utilized during the surge phase of progesterone synthesis, providing energy for the luteinizing fGCs before vascular network establishment. The LH(hCG)-Ras/Raf/Mek/Erk-RUNX1-Insulin signaling cascade plays a crucial role in inducing fGC energy storage. Moreover, supplementation of glucose effectively enhances glycogen reserves, leading to increased progesterone secretion in developing corpora lutea. This technique has shown promise in improving luteal function in mice, sheep, and humans, significantly enhancing reproductive performance.

RESULTS

1. Integrative analysis of single-cell and spatial transcriptomics revealed a decrease in metabolic activity in fGCs post-ovulation/luteinization stimulation

Ovaries were collected at 0 (H0), 1 (H1), and 6 hours (H6) post-hCG injection for single-cell RNA-seq. High-resolution transcriptomes of 12 types of ovarian cells,

including fGCs, were obtained through sequencing (Figure 1A, B). Subsequently, utilizing Tangram, we integrated the single-cell and ovarian spatial transcriptomic data acquired from public databases (see Materials and Methods), leading to the specific extraction of high-resolution transcriptome profiles of fGCs from preovulatory follicles post-hCG injection (Figure 1A). To delve into the cellular changes in fGCs during ovulation/luteinization, we performed Gene Ontology (GO) analysis on the genes upregulated by hCG, revealing their involvement in key biological processes such as *cell adhesion*, *motility*, *vascularization*, *inflammatory reactions*, *cell differentiation*, and *insulin receptor activity* (Figure 1C, D). These processes have been consistently observed in previous studies on ovulation/luteinization.

Our focus then turned to the downregulated gene cluster. GO analysis revealed a wide range of essential biological processes governed by the downregulated genes, including *Protein N-linked glycosylation*, *Protein palmitoylation*, *Protein homooligomerization*, *Protein homotetramerization*, *Protein folding*, *N-glycan processing*, *Protein O-linked mannosylation*, *endoplasmic reticulum stress*, *Oligosaccharide catabolic process*, *Protein localization*, *Lysosome organization*, , *Vesicle-mediated transport*, *Receptor-mediated endocytosis*, *Golgi-associated vesicle membrane*, *Transmembrane transport*, *Golgi apparatus*, *Respiratory chain complex I assembly*, *Mitochondrial membrane potential*, *Respiratory electron transport chain*, *Mitochondrial ATP synthesis*, *Aerobic respiration*, *Carbohydrate metabolic process*, *Tricarboxylic acid cycle*, *Superoxide metabolic process*, *Response to carbohydrate*, *Lipid metabolic process*, *Fatty acid beta-oxidation*, *Fatty acid metabolic process*, and *Triglyceride metabolic process* (Figure 1E, F). According to principles of cell biology, these processes either involve high-energy demanding metabolism in the endomembrane system or contribute to carbohydrate breakdown and ATP generation in the mitochondria and cytoplasm. Thus, the GO analysis of the downregulated genes unveiled a novel cellular response where fGCs shifted to an energy-saving mode upon exposure to ovulation/luteinization signals, reducing high-energy demanding metabolic activities, limiting ATP production, and curbing carbohydrate consumption.

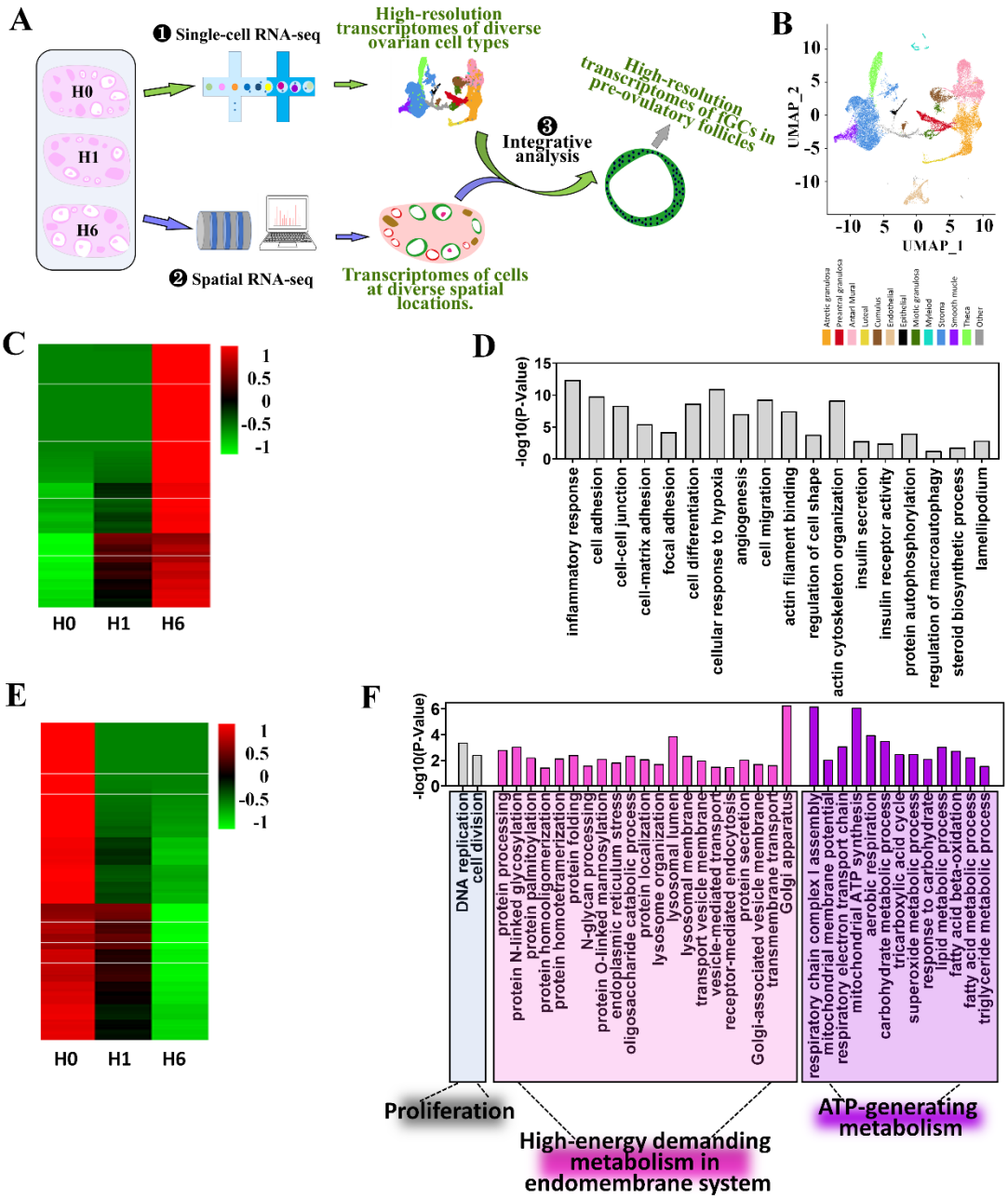

Figure 1. Integrative single-cell and spatial transcriptomics unveil reduced metabolic intensity in fGCs post-ovulatory stimulation. (A) Schematic illustrating the workflow for integrative analysis of single-cell and spatial transcriptomics. (B) UMAP of single cell RNA-seq identifies 12 cell types in ovaries. (C) Heatmap displaying genes from the upregulated expression cluster. (D) GO analysis of the upregulated expression cluster. (E) Heatmap presenting genes from the downregulated expression cluster. (F) GO analysis of the downregulated expression cluster.

2. Ovulation/luteinization signal attenuated metabolism and energy expenditure in fGCs

Next, experiments were conducted to verify decreased metabolic activity in fGCs as indicated by transcriptomic analysis. The endomembrane system, comprising the endoplasmic reticulum, Golgi apparatus, and lysosome, serves as the primary sites for high-energy demanding metabolism such as protein synthesis, glycosylation modification, vesicular transport, and membranous organelle assembly. Ultrastructural observation revealed enlarged endoplasmic reticulum tubules and an abundance of transport vesicles around the Golgi apparatus in fGCs before ovulation/luteinization stimulation. However, at 6h post-stimulation, the enlarged endoplasmic reticulum tubules transformed into cord-like structures and the number of transport vesicles around the Golgi apparatus decreased significantly (Figure 2A). qRT-PCR analysis further demonstrated a global downregulation of genes involved in oligosaccharide chain synthesis, N-linked glycosylation, vesicle assembly in the endoplasmic reticulum, and O-linked glycosylation in the Golgi apparatus following stimulation (Figure 2B). Genes associated with the M6P pathway controlling lysosomal assembly were also downregulated post-stimulation (Figure 2C). Flow cytometry analysis revealed a decrease in the proportion of fGCs with high Lyso-Tracker fluorescence intensity at H1 and H6 (Figure 2D). The activity of acid phosphatase, a lysosome-related functional enzyme, significantly decreased at H1 and H6 (Figure 2E).

Subsequent investigation focused on metabolic activities involved in energy production. Ultrastructural observation indicated a shift in mitochondria shape from round to oval post-ovulation/luteinization stimulation, along with a significant decrease in contact sites with the endoplasmic reticulum (Figure 2F). Contact with the endoplasmic reticulum is considered an indicator of active mitochondrial metabolism[33, 34]. Despite a notable rise in mitochondrial copy number (Fig. S1A), the mitochondrial membrane potential and ATP content significantly decreased while NAD^+/NADH ratio increased in fGCs post-stimulation (Figure 2G-I). These findings support the transcriptomic analysis, confirming reduced high-energy demanding

metabolism and decreased energy expenditure in fGCs following ovulation/luteinization stimulation.

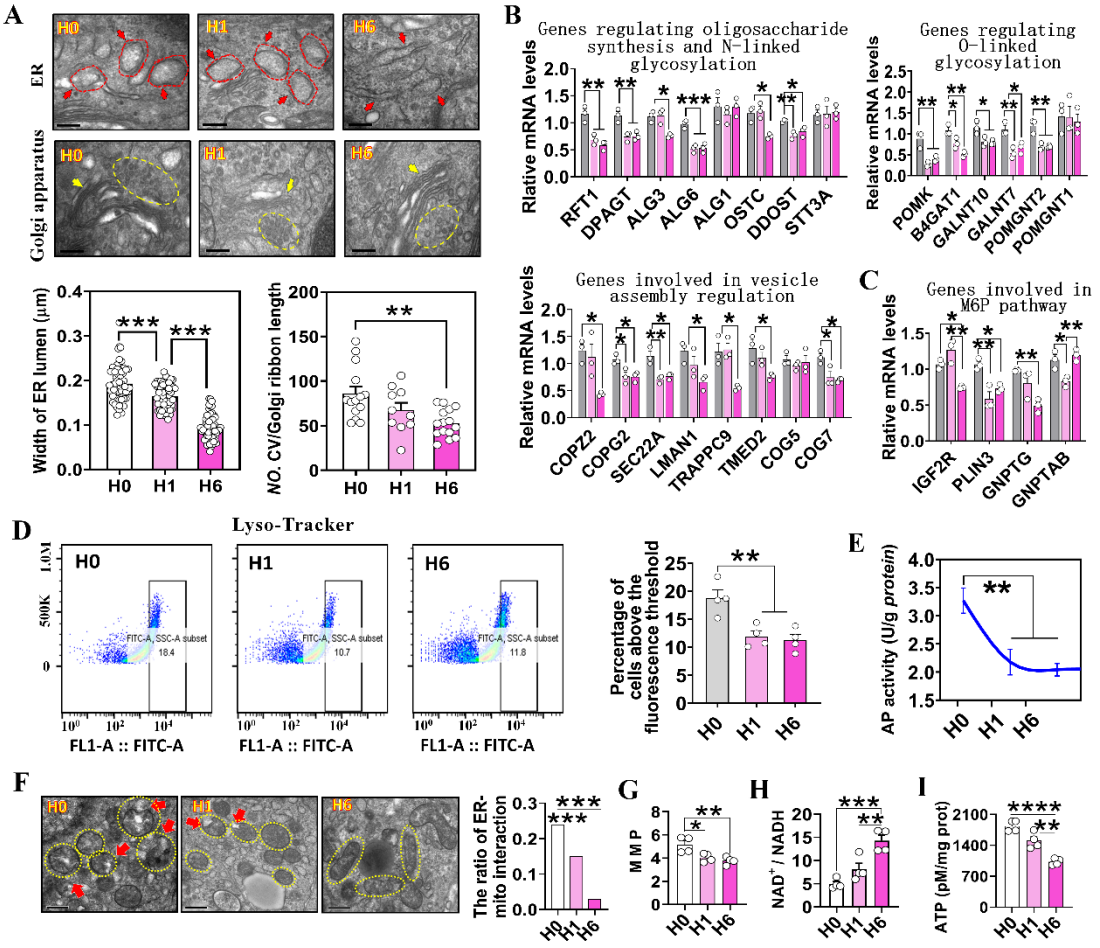

Figure 2. Impact of ovulation/luteinization signal on metabolism and ATP generation in fGCs. (A) Ultrastructural changes in ER and Golgi apparatus of fGCs following ovulation/luteinization stimulation. Up: Post-stimulation, ER transitioned from swelling to elongation (indicated by red arrow), with decreased transport vesicles surrounding the Golgi apparatus (yellow arrow); scale bar = 200 nm. Down: Statistical analysis based on 60 randomly selected ER structures and 10-15 Golgi apparatus structures *per* group. (B) Alterations in gene expression related to oligosaccharide biosynthesis, N-linked glycosylation, O-linked glycosylation and vesicle assembly post-ovulation/luteinization stimulation; n = 3 independent fGC samples. (C) Changes in expression of core genes in the M6P pathway post-ovulation/luteinization stimulation; n = 3 independent fGC samples. (D-E) Lysosomal changes following ovulation/luteinization stimulation. (D) Flow cytometry analysis showing reduced proportion of fGCs with high Lyso-tracker fluorescence post-stimulation; Representative images with fluorescence threshold indicated by red dotted line; n = 4 independent fGC samples. (E) Alterations in acid phosphatase activity post-stimulation; n = 4 independent fGC samples. (F-I) Changes in ATP production post-ovulation/luteinization stimulation. (F) Ultrastructural changes in mitochondria shape and ER contact sites post-stimulation; scale bar = 500 nm. (G) Mitochondrial membrane potential changes post-stimulation; n = 4 independent fGC samples. (H) NAD^+/NADH alterations post-stimulation; n = 4 independent fGC sample. (I) ATP

content variations post-stimulation; n = 4 independent fGC samples. Statistical significance were determined using one-way ANOVA followed by Tukey's post hoc test, values were mean ± SD. Significant differences were denoted by *P<0.05, **P<0.01, ***P<0.001, ****P<0.0001.

3. fGCs uptake glucose for conversion into glycogen reserves

Despite the decrease in metabolic intensity and energy expenditure post-ovulation/luteinization stimulation, flow cytometry analysis revealed an increased glucose uptake by fGCs (Figure 3A). The glucose transporter SLC2A1 was identified as the primary transporter responsible for this uptake, being the sole transporter expressed in fGCs and induced by hCG (Figure 3B, S2A-B). The elevated glucose uptake in fGCs amidst reduced energy expenditure is puzzling. According to biochemical principles, glucose entering the cell is either completely broken down to produce ATP, a possibility already eliminated by Figure 2F-I, or converted into other biomacromolecules such as lipids or glycogen (Figure 3C). Analysis ruled out lipid synthesis as the levels of free fatty acids and triglycerides decreased post-ovulation/luteinization stimulation (Figure S2C-D). Transcriptomic and Western blot analysis confirmed the induction of glycogen synthesis-related proteins by ovulation/luteinization signal (Figure 3D, S2E, S2F), colorimetric assay (Figure 3E) and Periodic Acid-Schiff (PAS) staining (Figure 3F) further confirmed a substantial increase in glycogen content in fGCs at H6, suggesting the glucose taken up by fGCs undergoes conversion into glycogen. Taken together, these findings unveil a novel reproductive phenomenon where fGCs swiftly transition to a low-energy state upon receiving ovulation/luteinization signals, minimizing metabolic intensity and energy expenditure while storing high levels of glucose as glycogen. We termed this phenomenon as "fGC energy storage".

To investigate the biological implications of fGC energy storage, we conducted an integrated analysis of the dynamics of glycogen storage and glycogenolysis, ATP generation, progesterone synthesis, and angiogenesis during ovulation/luteinization. Western blot (Figure 3G) and PAS staining (Figure 3H) showed that glycogen accumulation occurred from H0 to H9, followed by a consumption phase from H9 to H15. During the glycogen accumulation phase, ATP production significantly decreased (Figure 3I), while progesterone levels gradually increased below the 80ng threshold

(Figure 3J), during the glycogen consumption phase, ATP production sharply rose (Figure 3I), and progesterone levels exceeded 100ng/g, reaching approximately 200ng/g (Figure 3J). However, during the glycogen consumption phase characterized by heightened progesterone secretion and ATP demand, the developing corpora lutea exhibited an absence of an established vascular network internally (Figure 3K). Based on these observations, we speculate that the purpose of fGCs storing glycogen is to supply energy for intense progesterone production by the developing corpus luteum during the nonvascular phase.

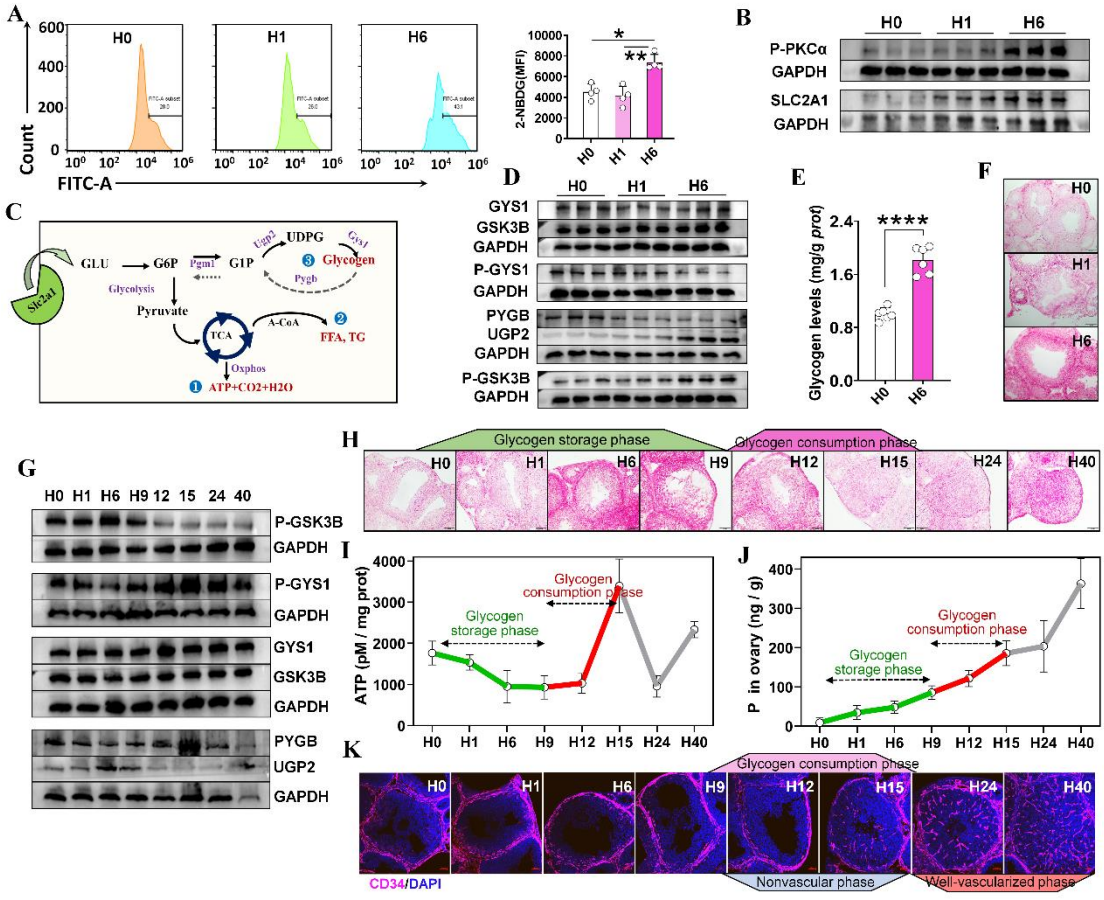

Figure 3. fGCs uptake glucose for conversion into glycogen reserves. (A) Flow cytometric analysis of glucose uptake capacity in fGCs post-ovulation/luteinization stimulation using the fluorescent glucose analog, 2-NBDG. Left: Representative images. Right: Statistical chart; n = 4 independent fGC samples. (B) Western blot analysis of SLC2A1 and its upstream kinase p-PKCα protein levels in fGCs post-stimulation. (C) Schematic representation of glucose carbon flux upon cellular entry. (D) Western blot depicted changes in proteins related to glycogen synthesis and degradation within 6 hours post-ovulation/luteinization stimulation. (E) Colorimetric measurement of glycogen content in fGCs within 6 hours post-stimulation; n = 6 independent fGC samples. (F) PAS staining for glycogen content in fGCs within 6 hours post-stimulation; scale bar = 100 μm. (G) Western blot analysis of protein levels associated with glycogen synthesis and degradation in fGCs within 40 hours post-

ovulation/luteinization stimulation. (H) PAS staining for glycogen content in fGCs within 40 hours post-stimulation; scale bar = 100 μm. (I) Changes in ATP content in fGCs within 40 hours post-stimulation; n = 4-7 independent fGC samples. (J) Progesterone content variations in ovarian homogenate within 40 hours post-stimulation; n = 4-7 independent ovarian samples. (K) Changes in vascular content within the fGC-layer within 40 hours post-stimulation, visualized by CD34 (red) as a vascular marker. Nuclei stained with DAPI (blue); scale bar = 50 μm. Statistical significance were determined using one-way ANOVA followed by Tukey's post hoc test (A) or two-tailed unpaired Student's t-test (E), values were mean ± SD. Significant differences were denoted by *P<0.05, **P<0.01, ****P<0.0001.

4. Mobilization of glycogen storage to support developing corpus luteum prior to vascularization

To test this speculation, 2g/kg dose of glucose was injected during glycogen storage phase to enhance glycogen storage in fGCs (Figure 4A), and its impact on luteal function was assessed. The results revealed that, at H6, glucose injection effectively increased glycogen storage in fGCs (Figure 4B, C). At H15, the expression level of luteal function-related genes in luteinizing fGCs with increased glycogen storage and the levels of progesterone in ovarian homogenates were significantly higher than those in the control group (Figure 4D, E). This enhancement of luteal function persisted until H40 (Figure S3A), coinciding with the full development of the vascular network, despite no significant difference in the number of corpora lutea between the two groups (Figure S3B).

Subsequently, an in vitro ovulation/luteinization induction system [17] was employed to knock down the expression of glycogen synthesis genes *Ugp2* and *Gys1* (Figure 4F, S3C, S3D). The results indicated a significant reduction in glycogen storage upon silencing these genes (Figure 4G). At H15, the knockdown group exhibited a substantial increase in NAD^+/NADH ratio (Figure 4H), as well as a notable decrease in mitochondrial membrane potential (Figure S3E), ATP content (Figure 4I), progesterone levels (Figure 4J), and the expression of luteal function-related genes (Figure S3F) compared to the control group. To further explore the impact of inhibited glycogen storage on luteal function in vivo, *Gys1* interference plasmids were injected into the ovarian bursa (Figure 4K-M, S3G). Consistent with the in vitro observations, *Gys1* knockdown led to a substantial increase in NAD^+/NADH ratio (Figure 4N) and a

decrease in ATP content (Figure 4O) in luteinizing fGCs. Additionally, there was a reduced expression of luteal function genes (Figure S3H) and diminished serum progesterone levels (Figure 4P). Conversely, we employed ingliforib, a PYGB inhibitor, to block glycogen breakdown during its consumption phase (Figure 4Q, R). The results showed that, compared with the control group, the developing corpus luteum with inhibited glycogenolysis had significantly lower ATP levels (Figure 4S), progesterone secretion (Figure 4T) and expression of luteal function genes (Figure S3I).

These findings support the hypothesis that fGCs store glycogen to fuel the developing corpus luteum during nonvascular phase.

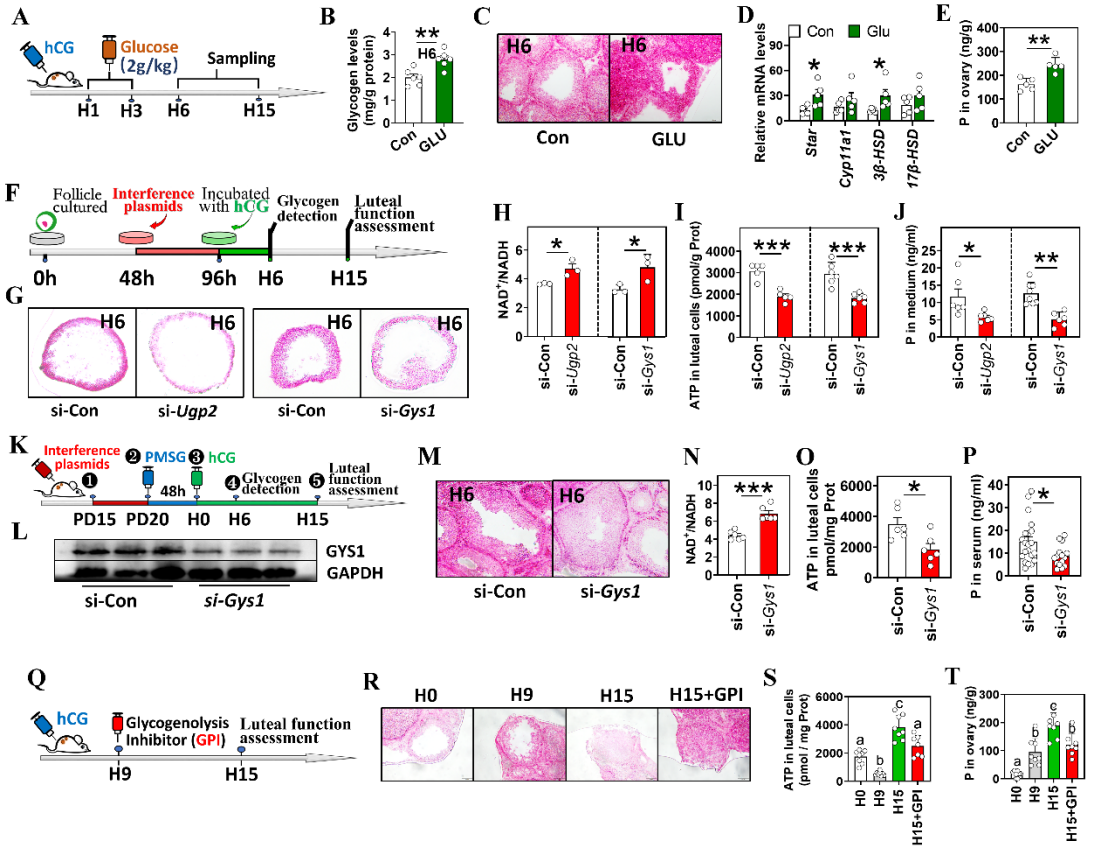

Figure 4. Mobilization of glycogen storage to support developing corpus luteum prior to vascularization. (A-E) Glucose injection during glycogen storage phase enhances mouse luteal function. (A) Experimental design for panels B to E. Luteinizing fGCs were isolated from developing corpus luteum at H15. (B) Colorimetric analysis of glycogen content in fGCs post-injection; n = 6 independent fGC samples. (C) PAS staining illustrated changes in fGC glycogen content post-injection; scale bar = 100 μm. (D) qRT-PCR analysis of gene expression related to luteal function in luteinizing fGCs post-injection; n = 5 independent fGC samples. (E) Radioimmunoassay measured progesterone levels in ovarian homogenates post-injection; n = 5 independent ovarian samples. (F-J) *Ugp2* and *Gys1* knockdown in cultured follicles impaired energy supply and progesterone production in developing corpus luteum. (F) Experimental design for

panels G to J, with scrambled shRNA serving as si-Control (si-Con). Luteinizing fGCs were isolated from the ruptured follicle at H15. (G) PAS staining showed changes in fGC glycogen storage post-*Ugp2* and *Gys1* knockdown; scale bar = 100 μm. (H) Alterations in NAD^+/NADH in luteinizing fGCs post-knockdown; n = 3 independent fGC samples. (I) ATP content variations in luteinizing fGCs post-knockdown; n = 5-6 independent fGC samples. (J) Radioimmunoassay measured progesterone levels in culture medium post-knockdown; n = 5-7 independent samples. (K-P) In vivo knockdown of ovarian *Gys1* affected energy supply and progesterone production in developing corpus luteum. (K) Experimental design for panels L to P, with luteinizing fGCs isolated from developing corpus luteum at H15. (L) Western blot confirmed *Gys1* knockdown in the ovary. (M) PAS staining indicated changes in glycogen content in fGCs post-knockdown; scale bar = 100 μm. (N) Alterations in NAD^+/NADH in luteinizing fGCs post-knockdown; n = 6 independent fGC samples. (O) Changes in ATP content in luteinizing fGCs post-knockdown; n = 6 independent fGC samples. (P) Serum progesterone level alterations post-knockdown; n = 21 (si-Con), 15 (si-*Gys1*) independent serum samples. (Q-T) Inhibiting glycogenolysis during glycogen consumption phase affected energy supply and progesterone production in luteinized fGCs. (Q) Experimental design for panels R to T.(R) PAS staining examined the inhibitory impact of GPI on glycogenolysis; scale bar = 100 μm. (S) Effect of inhibiting glycogenolysis on ATP levels in luteinizing fGCs; n = 7-8 independent fGC samples. (T) Impact of inhibiting glycogenolysis on progesterone levels in ovarian homogenates; n = 8 independent ovarian samples. Statistical significance was determined using two-tailed unpaired Student's t-test (B, D, E, H, I, J, N, O, and P) or one-way ANOVA followed by Tukey's post hoc test (S and T), values were mean ± SD. Significant differences were denoted by *$P < 0.05$, **$P < 0.01$, ***$P < 0.001$. (a–c) Different letters indicate a significant difference ($P < 0.05$).

5. The Ras/Raf/Mek/Erk-RUNX1-Insulin cascade mediated ovulation/luteinization signal-induced glycogen storage

To elucidate the signaling pathways governing fGC energy storage, we conducted an analysis of genes upregulated by hCG using Kyoto Encyclopedia of Genes and Genomes (KEGG) analysis. This analysis focused on the insulin signaling for regulating glucose homeostasis (Figure 5A). Building upon this finding, we postulated that hCG stimulates glucose uptake and glycogen storage through insulin signaling. Subsequent qRT-PCR and Western blot analyses confirmed that hCG significantly increased the mRNA levels (Figure S4A), protein levels, and phosphorylation status of insulin-related receptors (INSR and IGF1R) (Figure 5B). Furthermore (Figure 5C-E), the addition of insulin alone in the ovulation/luteinization induction system was adequate to upregulate the glucose transporter SLC2A1, enhance the glycogen synthesis enzymes GYS1 and GSK3B, promoting glucose uptake and glycogen storage in fGCs. Conversely, treatment with the INSR/IGF1R inhibitor BMS536924

353 completely blocked hCG-induced upregulation of SLC2A1 and enhancement of GYS1
354 and GSK3B activities, resulting in decreased glucose uptake and glycogen storage in
355 fGCs. These findings suggest that the ovulatory/luteinization signal stimulates fGC
356 energy storage by activating the insulin signaling pathway.

357 Subsequent investigation delved into the mechanism through which the
358 ovulatory/luteinization signal activates the insulin signaling. KEGG analysis of the
359 upregulated genes by hCG revealed a significant amplification of the MAPK
360 (Ras/Raf/Mek/Erk) kinase cascade post-ovulatory/luteinization stimulation (Figure
361 5A). Moreover, we identified RUNX1, a downstream transcription factor of the
362 Ras/Raf/Mek/Erk cascade, among the top 10 most induced transcription factors by hCG
363 (Figure 5F). Further analysis of ChIP-seq data from fGCs [32] indicated significant
364 binding peaks of RUNX1 in the promoters of *Insr* and *Igf1r* (Figure 5G). These
365 observations led us to propose that hCG activates insulin signaling through the
366 Ras/Raf/Mek/Erk-RUNX1 axis. Introducing C16-PAF, a Ras/Raf/Mek/Erk activator,
367 into the ovulation/luteinization induction system led to the upregulation of RUNX1,
368 INSR/IGF1R, p-INSR/IGF1R, SLC2A1 and glycogen storage even in the absence of
369 hCG. Conversely, inhibition of the Ras/Raf/Mek/Erk cascade with a specific inhibitor
370 U0126 prevented hCG-induced upregulation of RUNX1, INSR/IGF1R, p-INSR/IGF1R,
371 SLC2A1 and glycogen synthesis-related proteins (Figure 5H), resulting in the failure
372 of glycogen storage in fGCs (Figure 5I). To obtain direct evidence for the interaction
373 between RUNX1 and *Insr/Igf1r*, we employed both EMSA and ChIP-qPCR techniques
374 according the binding site predicted by JASPR database (Figure S4B, S4C and S4D).
375 The EMSA result revealed a distinct shifted band corresponding to the RUNX1-
376 Probe^{Insr,Igfr} (Figure 5J); ChIP-qPCR assay confirmed direct interaction between
377 RUNX1 and the promoter regions of *Insr* and *Igf1r*, with increased interactions
378 observed at H6 (Figure 5K). Furthermore, through site-directed mutagenesis, we
379 identified the specific motifs within the promoters of *Insr* and *Igf1r* that directly engage
380 with RUNX1 as *TGTGGT* (Figure S4E and 5L). Finally, *RUNX1* knockdown in
381 cultured follicles demonstrated a significant decrease in INSR/IGF1R, P-INSR/IGF1R,
382 and p-GSK3B levels, accompanied by an increase in p-GYS1 levels at H6. Notably,
383 *RUNX1* knockdown led to glycogen storage failure (Figure S4F and 5M).

Collectively, these findings strongly confirm that the LH (hCG)-RAS/RAF/Erk-RUNX1-Insulin signaling cascade plays an indispensable role in regulating fGCs energy storage.

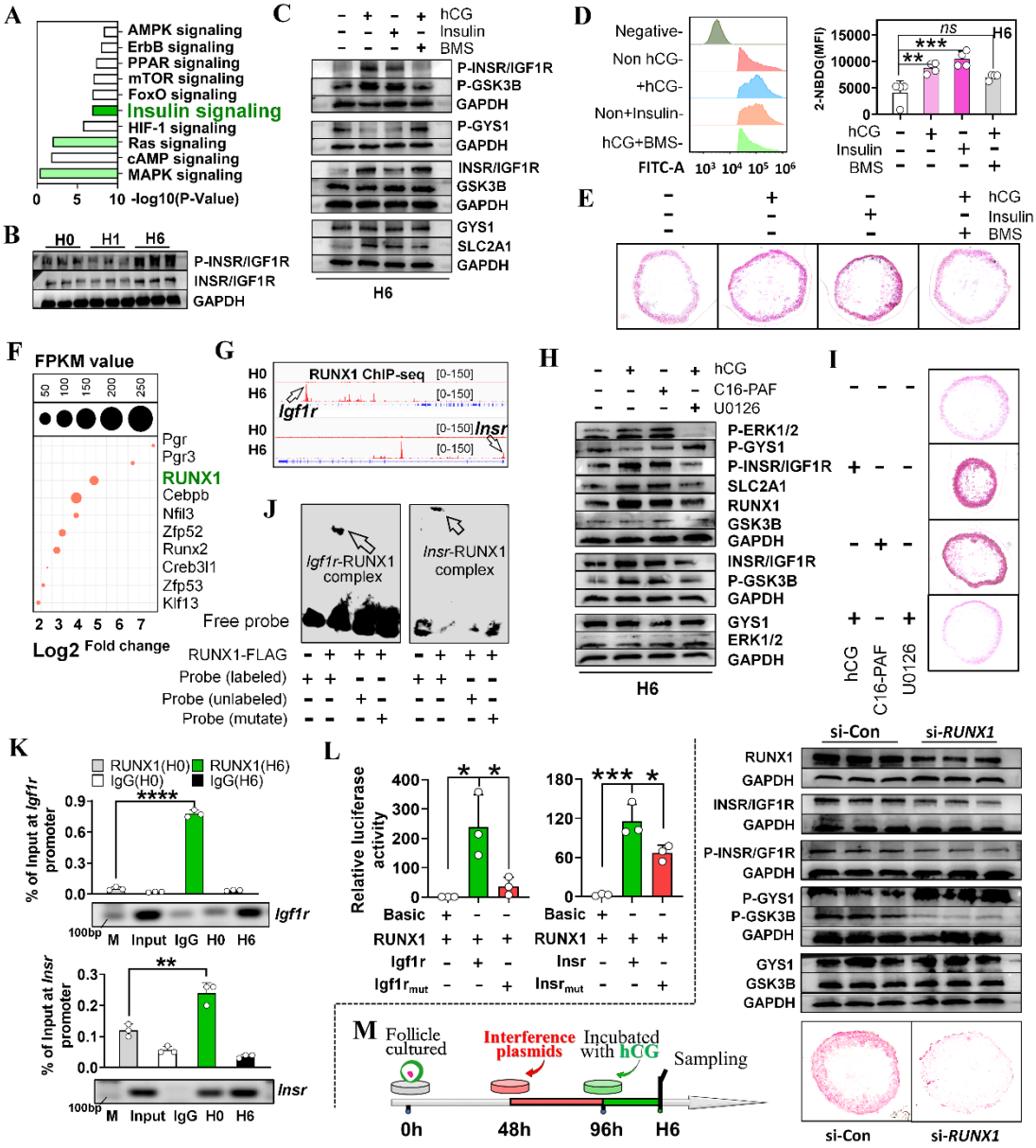

Figure 5. The Ras/Raf/Mek/Erk-Runx1-Insulin cascade in mediating ovulation/luteinization-induced glycogen storage. (A) KEGG analysis revealed activated signaling in fGCs post-ovulation/luteinization. (B) Western blotting displayed alterations in insulin receptor activity in fGCs post- stimulation. (C-E) Insulin signaling mediates hCG-induced glucose uptake and glycogen storage in fGCs. (C) Protein levels related to glucose uptake, glycogen synthesis, and glycogenolysis in fGCs were influenced by activation or inhibition of insulin signaling. (D) Flow cytometry measured changes in fGC glucose uptake capacity upon activation or inhibition of insulin signaling. Left: Representative images. Right: Statistical chart; n = 4 independent fGC samples. (E) Impact of activating or inhibiting insulin signaling on fGC glycogen content; scale bar = 100 μm. (F) Bubble plot of the top 10 transcription

factors significantly induced by hCG in fGCs. (G) ChIP-seq analysis revealed RUNX1 binding to *Insr* and *Igf1r* promoters. Arrows indicate RUNX1 binding peaks. (H) Effects of inhibiting or activating the Ras/Raf/Mek/Erk signaling cascade on RUNX1, glucose uptake-related, and glycogen synthesis-related protein levels in fGCs. (I) PAS staining illustrated the influence of inhibiting or activating Ras/Raf/Mek/Erk on fGC glycogen content; scale bar = 100 μm. (J) EMSA demonstrated RUNX1 binding to *Insr* and *Igf1r* promoter sequences. (K) ChIP-qPCR assay for RUNX1 binding to *Insr* and *Igf1r* promoters. Input and IgG are positive and negative controls, respectively. UP: qPCR statistical chart; n = 3 independent fGC samples. (L) Dual-luciferase reporter assay identified specific motifs within *Insr* and *Igf1r* promoters interacting with RUNX1; n = 3 independent samples. (M) Knockdown of *RUNX1* impacted glycogen synthesis-related protein levels and glycogen content in fGCs. Left: Experimental design. Right: Western blotting and PAS staining; scale bar = 100 μm. Statistical significance were determined using one-way ANOVA followed by Tukey's post hoc test, values were mean ± SD. Significant differences were denoted by *P<0.05, **P<0.01, ****P<0.001,****P<0.0001.

6. Elevation of glycogen storage through glucose administration enhanced luteal function and reproductive performance in mouse and ovine models.

To evaluate the clinical implications of fGC energy storage, we investigated whether enhancing this storage through glucose administration could enhance luteal function and reproductive outcomes in mice, sheep, and humans. Initially, we examined the impact of improved fGC energy storage on mouse reproductive performance under natural mating conditions. Glucose injections were administered at H1 and H3 (Figure 6A) to bolster glycogen storage (Figure 6B), with fetal number and development status assessed on day 15 of pregnancy (PD15). Results demonstrated a significant increase in progesterone levels on PD15 following glycogen storage enhancement (Figure 6C). Compared to the control group, the experimental group exhibited larger fetuses and a lower fetal regression rate, albeit with no significant change in the number of fetuses (Figure 6D). Subsequently, we evaluated the impact of enhanced glycogen storage on embryo transfer success rates (Figure 6E), revealing a notable improvement in the farrowing rate of transferred embryos compared to the control group (Figure 6F).

Moving on to sheep (Figure 6G), qRT-PCR and PAS staining suggested a significant increase in the expression levels of genes regulating glycogen metabolism (Figure 6H) and the storage of glycogen in sheep fGCs post-ovulation/luteinization stimulation (Figure 6I), indicating the conservation of fGC energy storage in sheep

(Figure 6H, I). Similar to mice, glucose injections post-ovulation/luteinization stimulation led to a significant boost in glycogen storage in sheep fGCs (Figure 6I). Subsequent assessment of luteal function on PD20 revealed a substantial increase in serum progesterone levels in the glycogen storage enhancement group compared to the control group (Figure 6J). Noteworthy, the pregnancy rate following breeding in the glycogen storage enhancement group reached 81.25% (Figure 6K), marking a significant 17.8 percentage point increase compared to the control group ($P<0.01$).

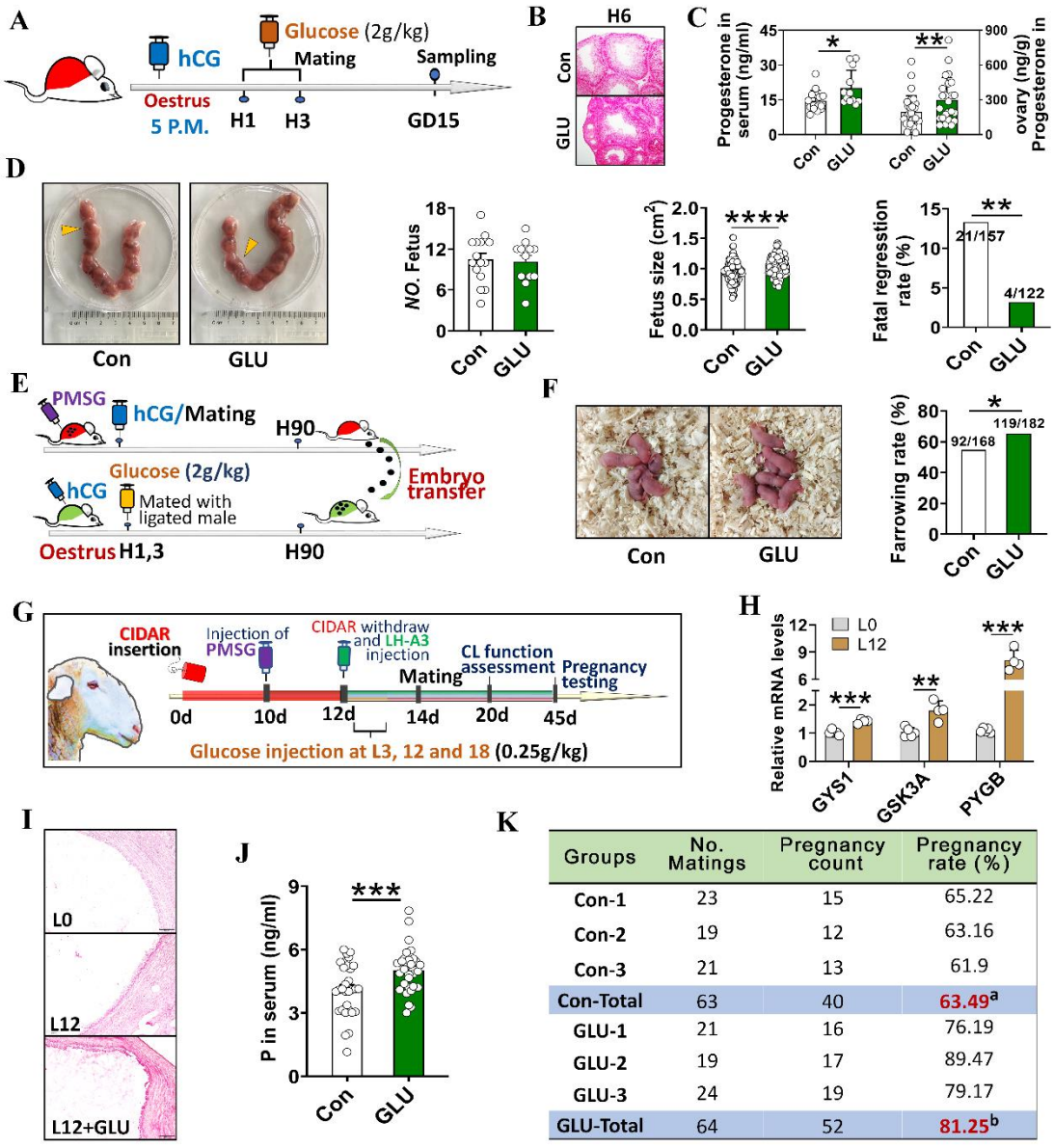

K

Groups	No. Matings	Pregnancy count	Pregnancy rate (%)
Con-1	23	15	65.22
Con-2	19	12	63.16
Con-3	21	13	61.9
Con-Total	63	40	63.49[a]
GLU-1	21	16	76.19
GLU-2	19	17	89.47
GLU-3	24	19	79.17
GLU-Total	64	52	81.25[b]

Figure 6. Elevation of glycogen storage through glucose administration enhanced luteal function and reproductive performance in mouse and ovine models. (A-D) Impact of glucose administration on mouse fetus development. (A) Experimental design for panels B to D. (B) PAS staining; scale bar = 100 μm. (C) Effects of glucose administration on progesterone levels in serum and ovarian homogenates of mice at

PD15; n (serum) = 15 (Con), 12 (GLU); n (ovarian homogenate) = 30 (Con), 24 (GLU). (D) Effects of glucose intake on the number, size, and regression rate of fetuses at PD15; n = 15 pregnant mice. (E-F) Impact of glucose administration by recipient mice on farrowing rate of transferred embryos. (E) Experimental design. (F) Farrowing rate statistics of transplanted embryos. (G-K) Improvement in luteal function and pregnancy rate in sheep through glucose intake post-ovulation/luteinization stimulation. (G) Experimental design for panels H to K. (H) qRT-PCR analysis of ovulation/luteinization signal effects on glycogen metabolism-related gene expression in luteinized sheep fGCs; L12 indicates 12 hours post-LH injection; n = 5 (L0), 4 (L12) fGC samples. (I) PAS staining illustrated the impact of glucose intake on glycogen content in luteinized sheep fGCs; scale bar = 500 μm. (J) Effects of glucose intake on serum progesterone levels (n = 30 serum samples). (K) Effects of glucose intake on sheep pregnancy rate after breeding. Statistical significance were determined using two-tailed unpaired Student's t-test or chi-square test (the farrowing rate and pregnancy rate), values were mean ± SD. Significant differences were denoted by *P<0.05, **P<0.01, ***P<0.001, ****P<0.0001.

7. Elevation of glycogen storage through oral glucose enhanced human luteal function

Transitioning to human studies, we obtained down-regulated genes in human fCGs following ovulatory/luteinization stimulation from public databases. Similar to findings in mice, GO analysis revealed enrichment of these genes in high-energy demanding and ATP production processes (Figure 7A). Conversely, glucose transporters *SLC2A13*, *SLC2A14*, and *SLC2A3* exhibited a sharp increase 12h post-ovulatory/luteinization stimulation, returning to baseline levels after 32h (Figure 7B). Additionally, insulin signaling-related genes, including *IGF1R*, *IGFBP1*, *IGFBP3*, *IGFBP5*, and *IRS2*, were upregulated by ovulatory/luteinization stimulation (Figure 7C). qRT-PCR analysis further confirmed significant upregulation of glycogen metabolism genes *Gys1* and *PYGB* 36h post-stimulation (Figure 7D), suggesting the conservation of fCG energy storage in humans.

Subsequently, volunteers undergoing assisted reproductive treatment were recruited, with a requirement to orally ingest 75g glucose at H12. The progesterone synthesis capacity of luteinized fGCs was evaluated 24h following glucose ingestion (Figure 7E). Oral glucose intake significantly enhanced glycogen storage in human fGCs (Figure 7F). Compared to the control group, the experimental group exhibited a notable upregulation of progesterone synthesis-related gene expression in luteinized

fGCs (Figure 7G), leading to a 2.6-fold increase in the average progesterone content in follicular fluid (P<0.01) (Figure 7H). These results suggest that a single oral administration of glucose during the glycogen storage window can substantially improve human luteal function.

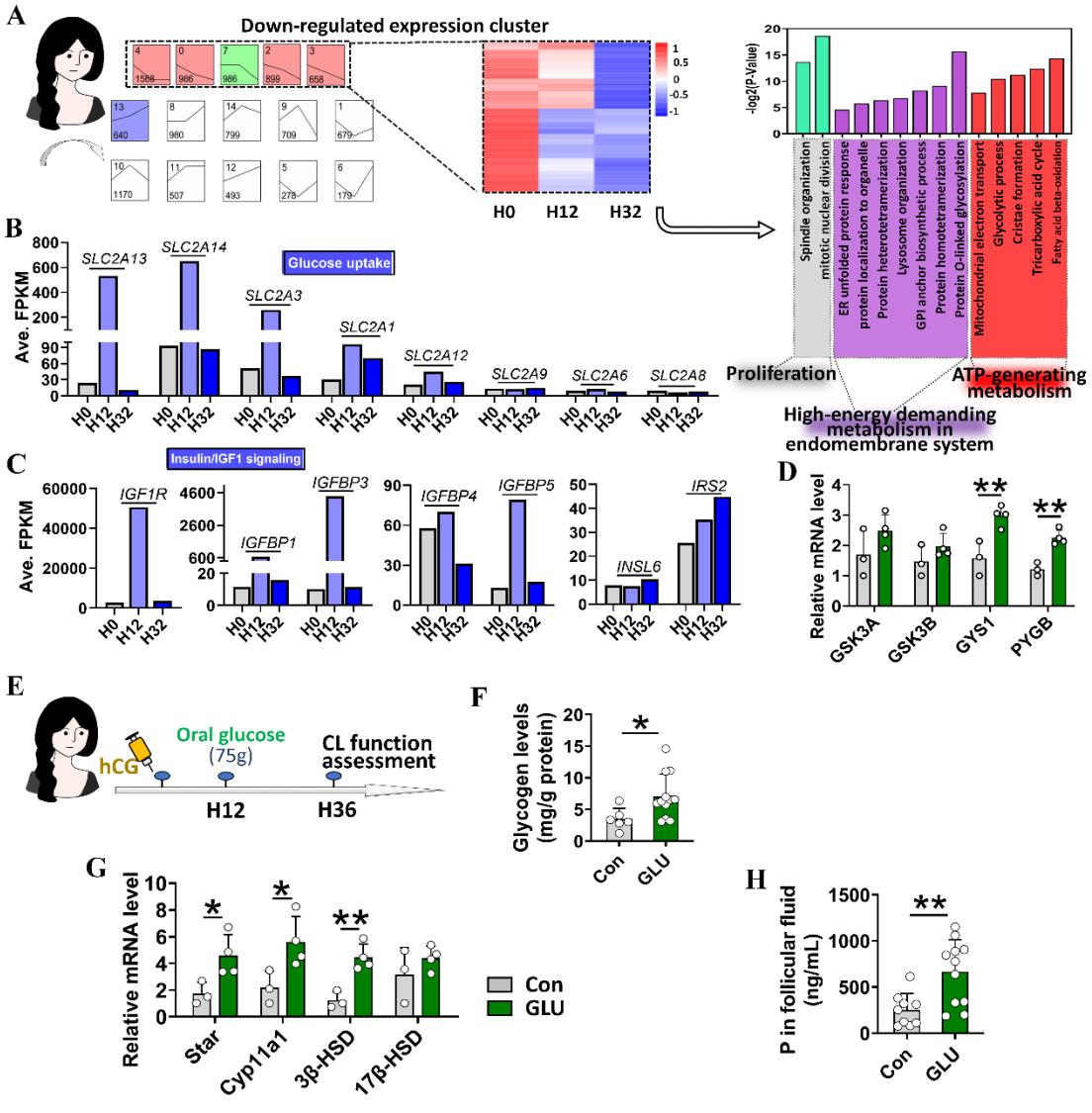

Figure 7. Elevation of glycogen storage through oral glucose enhanced human luteal function. (A-C) Bioinformatic analysis of the human fGC transcriptome post ovulation/luteinization stimulation. (A) GO analysis of the down-regulated gene cluster enriched with biological events related to high-energy demanding metabolism and ATP generation. (B) Expression of key genes involved in glucose uptake. (C) Expression of key genes in the Insulin/IGF1 pathway. (D) qRT-PCR analysis of the effects of ovulation/luteinization signal on the expression of genes related to glycogen metabolism in luteinized human fGCs; n = 3 (H0), 4 (H12) fGC samples. Luteinized fGCs were obtained from pre-ovulatory follicles of human subjects. (E-H) Oral glucose intake after ovulatory stimulation increased glycogen reserves and progesterone synthesis capacity in luteinized fGCs. (E) Experimental design for panels F to H. Volunteers were randomly selected from women undergoing IVF treatment and

responding normally to controlled ovarian hyperstimulation. (F) Colorimetric determination of the effects of oral glucose on glycogen content in luteinized human fGCs; n = 6 (Con), 13 (GLU) fGC samples.(G) qRT-PCR analysis of the effects of oral glucose on the expression of luteal function genes in luteinized fGCs from humans; n = 3 (Con), 4 (GLU) independent fGC samples. (H) Radioimmunoassay measuring changes in progesterone levels in human follicular fluid following glucose intake; n = 9 (Con), 11 (GLU) independent samples. Statistical significance were determined using two-tailed unpaired Student's t-test, values were mean ± SD. Significant differences were denoted by *P<0.05, **P<0.01.

DISCUSSION

The differentiation of fGCs into luteal cells, known as luteinization, involves a prolonged process characterized by a sharp increase in progesterone synthesis and the development of a robust vascular network to support this increase with sufficient energy and substrates.[35, 36] However, the increase in progesterone synthesis precedes the establishment of the vascular network, resulting in a period during which luteinizing fGCs experience a lack of blood supply.[37, 38] The mechanism by which these fGCs acquire sufficient energy supply for the increase in progesterone synthesis remains unclear. This study introduces the concept of fGC energy storage to elucidate this conundrum. Upon receiving the ovulation/luteinization signal, fGCs swiftly transition to an energy-saving mode, reducing their high-energy demanding metabolism. Simultaneously, them uptake significant amounts of glucose, storing it as glycogen. The stored glycogen is subsequently utilized during the avascular period, providing energy for the luteinizing fGCs (Figure 8).

The concept of fGC energy storage has significant theoretical implications. In the follicle, oocytes exhibit a strategy of material storage by halting their cell cycle in prophase to gather nutrients and signaling molecules, eventually becoming the largest cells in the organism.[39, 40] The discovery of fGC energy storage suggests that similar to oocytes, fGCs are also endowed with the behavior of material storage. The only difference is that, unlike oocytes which store a variety of substances for pre-implantation embryogenesis, fGCs specifically store glycogen to support luteinizing fGCs during the avascular phase.[41, 42] Taken together, the concept of fGC energy

storage enhances our comprehension of ovulation/luteinization. It is particularly noted that despite prior observations of glycogen in follicular cells, the active glycogen storage by fGCs and its role in folliculogenesis have not been extensively explored.[43, 44] Additionally, in metabolic research, hepatocytes and skeletal muscle cells are renowned for glycogen storage.[45, 46] Our study sheds light on fGCs as a new cell type actively storing glycogen, with glycogen storage in fGCs also regulated by insulin signaling, aligning with hepatocytes. Therefore, the discovery of fGC energy storage represents a notable advancement in metabolism research. Notably, unlike hepatocytes that synthesize both glycogen and fat [47], fGCs prioritize glycogen storage over fat. We posit that this preference aims to prevent damage from reactive oxygen species, as fat breakdown yields reactive oxygen species, while glycogenosis does not.

fGC energy storage presents notable clinical implications as a conserved cellular phenomenon observed across mice, sheep, and humans. In this study, we enhanced glycogen reserves through exogenous glucose administration, leading to a significant improvement in luteal function in mice, sheep, and humans. This technique, characterized by its simplicity and safety, solely requires glucose intake without the need for additional medications. Notably, the approach shows promising potential in enhancing reproductive performance, evidenced by increased fetal weight in mice, reduced fetal regression rates, and a marked improvement in live birth rates from transplanted embryos. Moreover, it notably raised the average pregnancy rate in naturally mated sheep by nearly 18 percentage points. While assessing the impact of luteal function enhancement technique on human pregnancy rates poses challenges, the discovery of fGC energy storage and the subsequent development of the luteal function enhancement technique offer new avenues for human fertility preparation. The prospect of enhancing the likelihood of conception simply by oral glucose intake holds appeal for individuals seeking pregnancy. Crucially, the success of the luteal function enhancement technique hinges on the strategic approach to glucose intake. Timing, frequency, and dosage of glucose consumption must be carefully optimized, with

ingestion during the glycogen storage window being essential as fGCs exhibit enhanced glucose transporter expression and activate glycogen synthesis pathways solely during this phase. Exploration of the optimal number of intake instances, intervals, and doses during this window necessitates thorough clinical validation.

Currently, this study has technical limitations. For future investigations, we will also employ metabolic flux analysis and ^{13}C isotope tracing techniques to provide direct evidence of glycogen synthesis in fGCs using glucose. Additionally, we have successfully conducted the specific knockout of *Gys1* in fGCs and intend to utilize the conditional *Gys1* knockout mouse model to assess the impact of inhibiting fGC energy storage on luteal function and reproductive performance. The materials and methods employed in this study will be thoroughly described in the finalized submission version.

In conclusion, this study introduces the innovative concept of fGC energy storage" and establishes the Luteal Function Enhancement Technique based on this theoretical framework. These findings contribute to the theoretical foundations of reproductive physiology and metabolism, highlighting their significant clinical relevance in enhancing mammalian reproductive performance.

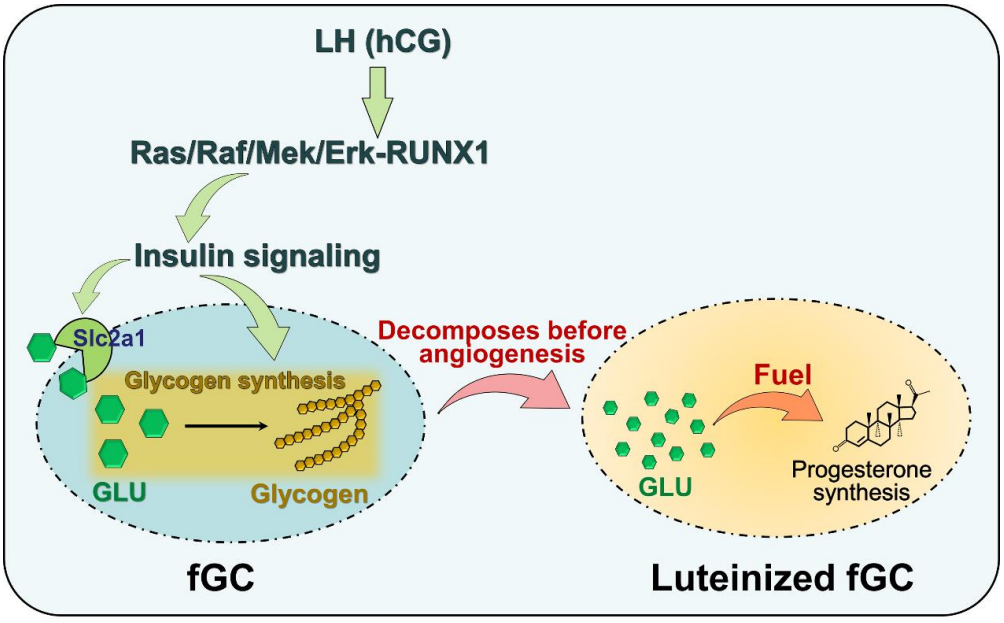

Figure 8. A diagram depicting ovulation/luteinization signal induced fGC energy storage.

MATERIALS AND METHODS

Animals

KM-strain mice were purchased from the Center for Animal Testing of Huazhong Agricultural University. Mice were reared in SPF laboratory animal house and were kept at a constant temperature of 22-26 °C, with a light/dark cycle of 12/12 hours, and allowed access to food and water ad libitum. The sheep were raised at the Xinjiang Jinken aoqun agriculture and animal husbandry technology Co., LTD, China. All experiments and handling of mice and sheep were conducted following the guidelines of the respective animal experimental institutions. Prior approval from the Institutional Animal Ethics Committee of Huazhong Agricultural University was obtained.

Human clinical trials

Female patients aged between 25 and 40 years, who were seeking in vitro fertilization (IVF) treatment, were enrolled as volunteers in this study. Informed consent was obtained from all participants after they were fully informed about the study's nature, purpose, potential risks, and benefits. 12 hours after hCG injection to induce ovulation/luteinization, each participant orally received glucose at a dose of 2 g/kg. Approximately 36 hours post-hCG injection, corresponding to the expected time of ovulation, follicular fluid and luteinized fGCs were extracted from the pre-ovulatory follicles. Sample preparation followed established protocols as described in the relevant literature [48]. The fGCs were utilized to evaluate glycogen storage and expression of luteal function-related genes, while the fluids were used to measure progesterone levels. Throughout the study, strict ethical considerations were observed to protect the participants' well-being and rights. Approval was obtained from the Ethics Committee of Renmin Hospital of Wuhan University, China, ensuring compliance with all ethical standards.

Superovulation

Mice were injected with 5 IU PMSG (NSHF, China) to stimulate follicle growth. 48 hours later, 5 IU hCG (NSHF, China) was injected to trigger ovulation/luteinization. In sheep, vaginal plugs containing progesterone (Zoetis Australia Pty Ltd, New Zealand) were inserted to synchronize estrous cycles. On day 10 after plug insertion, 400 IU

PMSG (NSHF, China) was injected. The plugs were removed 12 days after insertion, and simultaneously, 12.5 μg LH-A3 (NSHF, China) was injected to trigger ovulation/luteinization. Glucose was then subcutaneously injected at 0.25 g/kg at 3 h, 12 h and 18 h post-LH-A3 injection. The animals were subsequently bred, and luteal function was assessed on day 6 post-breeding. Pregnancy rates were determined one month later.

Integrative analysis of single-cell and spatial transcriptomics, analysis of RNA-Seq

Mouse ovaries were collected at H0, H1 and H6 for single-cell RNA-seq, which was conducted by Yingzi Gene (Wuhan, China). Initially, the cell number and viability were assessed, followed by loading cells onto the 10X Chromium Single Cell Platform (10X Genomics) at a concentration of 1,000 cells per μl. The protocol included the generation of gel beads in emulsion (GEMs), barcoding, GEM-RT clean-up, cDNA amplification, and library construction per the manufacturer's instructions. Library quantification was performed using Qubit before pooling, and the final library pool was sequenced on the Illumina Nova6000 platform using 150-base-pair paired-end reads. Subsequently, quality control and read counting of Ensembl genes were conducted using the cellranger software with default parameters (v2.1.0). Normalization, dimensionality reduction, and clustering of single cells were also accomplished using cellranger. To reduce dimensionality, the top ten principal components were utilized, and t-Distributed Stochastic Neighbor Embedding (tSNE) was employed. Cell clustering was achieved through a graph-based clustering algorithm, involving the construction of a sparse nearest-neighbor graph followed by Louvain Modularity Optimization.[49] Differential expression analysis between cell groups was performed using the Seurat-Bimod statistical test with significance set at FDR <= 0.05 and |log2 Fold Change| >= 1.5.

The spatial transcriptome data of mouse ovaries, contributed by Mantri et al[50], was extracted from the Gene Expression Omnibus database (Login Number: GSE240271). Spatial transcriptomics datasets, processed metadata, and cell annotations files were sourced from GitHub (https://github.com/madhavmantri/mouse_ovulation). The categorization of pre-ovulatory follicles and labeling of fGCs were completed by Mantri et al. Integration of

637 the 10× Single-cell and Spatial transcriptome datasets was carried out using the
638 Tangram package[51].
639 Human transcriptome data was extracted from the Gene Expression Omnibus
640 database, with login numbers GSE133868. STEM software was used to study the
641 expression profile of genes between time points. GO enrichment analysis of genes was
642 performed through DIVAD database (https://david.ncifcrf.gov/tools.jsp). KEGG
643 enrichment analysis of genes were performed through KOBAS database
644 (http://kobas.cbi.pku.edu.cn/home.d).

645 **Quantitative real-time PCR**

646 Total RNA was extracted using TRIzol reagent (Takara, 9109, Japan) following the
647 manufacturer's instructions. Reverse transcription was carried out by employing the
648 Evo M-MLV RT Kit (AGbio, AG11728, China). qRT-PCR analysis was performed
649 using a CFX384 Real-Time PCR System (Bio-Rad). The reaction mixture consisted of
650 5 μl SYBR Green (AGbio, AG11739, China), 4 μl cDNA template, 250 nM each of
651 forward and reverse primers, and ddH_2O to reach a total volume of 10 μl. Reaction
652 conditions included initial denaturation at 95 ℃ for 10 minutes, followed by 35 cycles
653 of denaturation at 95 ℃ for 10 seconds and annealing/extension at 60 ℃ for 30 seconds.
654 A final step involved a melting curve analysis spanning 60 ℃ to 95 ℃, with a 0.5 ℃
655 increment every 5 seconds. Relative RNA expression levels were determined using the
656 Ct ($2^{-\Delta\Delta Ct}$) method [52]. Amplified products were visualized through agarose gel
657 electrophoresis (80V, 80 mA, 75 minutes). The primer sequences utilized for PCR
658 amplification are provided in Table S1.

659 **Follicle culture**

660 Follicles were isolated and cultured following established procedures [53]. In brief,
661 follicles with a diameter of 250-300 μm were obtained from the ovaries using 33-gauge
662 microneedles (KONSFI, China). These follicles were then cultured in 96-well plates
663 (BKMAM, China) and placed in a 37°C incubator with 5% CO_2. The culture medium
664 comprised α-MEM (Gibco, C12571500BT, USA) supplemented with 1% ITS-G
665 (Macklin, I917634, China), 5% FBS (Serana, FBS-AS500, Germany), 10 mIU/mL FSH

(NSHF, China), and 100 U/mL penicillin/streptomycin (Servicebio, G4003, China). After 96 hours of culture, follicles that reached the pre-ovulatory stage (450-550 μm) were transferred to ovulation/luteinization medium and cultured for up to 15 hours. The ovulation/luteinization medium consisted of α-MEM supplemented with 1% ITS-G, 5% FBS, 10 mIU/mL FSH, 1.5 IU/mL hCG (NSHF, China), 10 ng/mL EGF (PeproThec, AF-100-15, USA), 5mg/mL D-Glucose (MCE, HY-B0389, USA), 1ng/mL Prolactin (MCE, USA), 10 μM Cholesterol (MCE, USA), and 100 U/mL penicillin/streptomycin.

RNA interference

Lentivirus-mediated RNA interference was employed to silence gene expression in follicles or ovaries. Interference vectors were constructed using the PLKO.1-EGFP-PURO plasmid (Genecreate, China). Small interfering RNAs (siRNAs) targeting *Gys1*, *Ugp2*, and *RUNX1* were synthesized by Genepharma (China), with the following sequences: *Gys1* - 5′- gcccatgtcttcactaccgta-3′, *Ugp2* - 5′- gcaaactgagactggtggaaa-3′, *RUNX1* - 5′- cggcagaactgagaaatgcta-3′. A scrambled shRNA with the sequence 5′-caacaagatgaagagcaccaa-3′ served as a negative siRNA control. Lentivirus was packaged in 293T cells (ATCC, USA) by co-transfecting three vectors: 0.89 μg PLKO.1-EGFP-PURO, 0.44 μg of pMD2.G (Addgene, USA), and 0.67 μg of pSPAX2 (Addgene, USA) using 4 μl jetPRIME® (PolyPlus-transfection, 101000046, France) in each well of a six-well plate. After 48 hours, the viral supernatants were harvested, centrifuged, and filtered through 0.45 μm polyvinylidene fluoride (PVDF) membranes (Sigma-Aldrich, SLHVR33RB, USA).

For lentivirus infection of cultured follicles, 100 μl of lentivirus (titer: 1.25×10^8 viral particles/mL) and 1 μg of polybrene were added to each milliliter of medium. For in vivo ovary infection, 15-day-old mice were anesthetized with pentobarbital sodium (1%). Subsequently, 5 μl of lentivirus (titer: 1.25×10^9 viral particles/mL) was injected into the ovarian bursa using a 10μl syringe (Hamilton, Switzerland) and a 33-gauge Small Hub RN Needle (Hamilton, Switzerland). Follow-up experiments were conducted on these mice 6 days after plasmid transfection.

Western blot

Total proteins were extracted using RIPA lysis buffer (ComWin Biotech, CW2333S, China) supplemented with protease and phosphatase inhibitors (ComWin Biotech, CW2383S, China) and PMSF (Solarbio, P0100, China). The protein concentration was determined using the BCA Protein Assay Kit (Servicebio, G2026, China). Subsequently, the proteins were separated by polyacrylamide gel electrophoresis and transferred onto a polyvinylidene fluoride membrane (Sigma-Aldrich, IPVH00010, USA). After transfer, the membrane was blocked with 5% skim milk powder (Nestle, Switzerland) at room temperature, followed by overnight incubation at 4°C with specific primary antibodies: P-PKCα (1:1000 dilution; 9375T, CST, USA), SLC2A1 (1:1000 dilution; 21829-1-AP, Proteintech, USA), GYS1 (1:1000 dilution; 3886T, CST, USA), GSK3B (1:1000 dilution; 12456T, CST, USA), P-GYS1 (1:1000 dilution; 47043T, CST, USA), P-GSK3B (1:1000 dilution; 9323T, CST, USA), PYGB (1:1000 dilution; 12075-1-AP, Proteintech, USA), UGP2 (1:800 dilution; 10391-1-AP, Proteintech, USA), INSR/IGF1R (1:1000 dilution; A21984, Abclonal, China), P-INSR/IGF1R (1:800 dilution; 3024T, CST, USA), RUNX1 (1:1000 dilution; 25315-1-AP, Proteintech, USA), ERK1/2 (1:1000 dilution; A4782, Abclonal, China), P-ERK1/2 (1:1000 dilution; AP0234, Abclonal, China), GAPDH (1:5000 dilution; AC002, Abclonal, China). The membrane was then washed three times with TBST (Solarbio, China) and incubated with the appropriate HRP-conjugated secondary antibodies (goat anti-rabbit secondary antibody, 1:4000 dilution, BF03008; goat anti-mouse secondary antibody, 1:4000 dilution, BF03001, Biodragon-immunotech, China) for 1 hour at room temperature. Following further washing with TBST, the protein bands were visualized using an ECL chemiluminescent reagent kit (Biosharp, BL520A, China). Image capture was carried out with a Chemiluminescence imager (Tannon-5200, China). The original blots can be viewed in Fig. S5.

Immunofluorescence staining

Ovaries were fixed in 4% paraformaldehyde (Servicebio, G1101, China), and then embedded in paraffin. Sectioning of ovaries were performed and thick of sections was

3 μm. Subsequently, the sections were deparaffinized and rehydrated, followed by high-temperature antigen retrieval at 95-98 °C for 25 minutes using a 5% antigen retrieval buffer (Solarbio, C1032, China). Next, the sections were blocked with goat serum (10%) (Boster, AR0009, China) for 1 hour at room temperature. Next, the sections were incubated with the primary antibody CD34 (1:300 dilution; A19015, Abclonal, China) for 16 h at 4 °C. After washing, the slices were incubated with ABflo® 594 -conjugated secondary antibody (1:200 dilution, AS039, ABclonal, China) for 60 min at room temperature. Finally, the slices were stained with DAPI (Biosharp, BS097, China). Following another round of washing, the sections were imaged using an LSM800 confocal microscope system (Zeiss, Germany) and the resulting images were analyzed using Zen 2.3 lite software.

Transmission electron microscope

Pre-ovulatory follicles isolated from the ovaries were utilized for transmission electron microscopy analysis following standard procedures. The follicles were immersed in 2.5% (v/v) glutaraldehyde fixative (SPI Chem, USA) at 4°C overnight for initial fixation. Subsequent to fixation, the samples were rinsed with PBS and treated with a 1% osmic acid solution (SPI Chem, USA) for 2 hours. Following this, the samples were dehydrated using a gradient acetone (Sinopharm, China) series and infiltrated with a gradient Spurr resin-acetone solution (SPI Chem, USA). The samples were then polymerized with pure Spurr resin (SPI Chem, USA) at 60°C for 48 hours. Ultrathin sections of 60 nm thickness were cut using an ultramicrotome (Leica, USA) and collected onto copper grids. The sections were stained with a 2% uranium acetate solution (w/v) (SPI Chem, USA) for 30 minutes. The ultrastructure of fGCs was visualized using a transmission electron microscope (HITACHI, JPN) operated at 80 kV, and observation results were captured using a CCD camera (Gatan, USA).

Flow cytometry

To assess lysosome content in fGCs using flow cytometry, Lyso-Tracker Green (Beyotime, C1047S, China) was utilized for lysosome labeling. Following the manufacturer's protocol, fGCs were initially washed with HBSS (Beyotime, C0219,

752 China). Subsequently, the cells were stained with the Lyso-Tracker Green working
753 solution and incubated at 37 °C for 30 minutes. Fluorescence values were measured
754 using a flow cytometry instrument (BD Biosciences, USA), and data analysis was
755 conducted through FlowJo 10.4 software (BD Biosciences, USA) following the
756 software's manual.

757 For evaluating glucose uptake capacity in fGCs, the fluorescent glucose analog 2-
758 NBDG (MCE, HY-116215, USA) was employed to track glucose internalization by
759 fGCs. Post-collection, the fGCs underwent two washes with PBS, followed by
760 resuspension in the 2-NBDG working solution. After a 30-minute incubation at 37°C,
761 the cells were washed twice with PBS, and the mean fluorescence intensity was
762 measured using a flow cytometry instrument (BD Biosciences, USA). Data analysis
763 was performed using FlowJo 10.4 software (BD Biosciences, USA).

764 **Enzyme activity analysis**

765 The activity of acid phosphatase was determined using Acid Phosphatase (ACP)
766 Activity Assay Kit (Boxbio, AKFA017C, China). fGCs supernatant was prepared and
767 incubated with ACP working solution, and then the absorbance at 510 nm was measured.
768 Enzymatic activities were converted from the respective absorbance and normalized by
769 the total protein amount.

770 **Mitochondrial membrane potential assay**

771 The mitochondrial membrane potential of fGCs was assessed utilizing the
772 Mitochondrial Membrane Potential Assay Kit with JC-1 (Solarbio, M8650, China).
773 Following the manufacturer's protocol, the fGCs were treated with JC-1 working
774 solution and incubated at 37°C for 20 minutes. Subsequently, the fGCs were washed
775 with staining buffer to eliminate surface fluorescence. The intensity of red and green
776 fluorescence was measured using a microplate reader (PerkinElmer, USA), and the ratio
777 of red to green fluorescence was utilized to calculate the mitochondrial membrane
778 potential.

779 **mtDNA copy number analysis**

780 Total DNA was extracted from fGCs using a mouse direct PCR Kit (KBD-BIO, B40013,

China), and used for the detection of mtDNA copy number by quantitative PCR. The mtDNA was amplified using primers targeting mitochondrial *MT-ND5*, and as a reference for normalization of mtDNA, the nuclear *Act-b* was amplified. The procedure of quantitative PCR was as follows: 95 °C for 15 min; 35 cycles of 95 °C for 10 s and 60 °C for 30 s; melting curve from 65 °C to 95 °C, increasing in an increment of 0.5 °C every 5 s. The primer sequences were listed in Table S1.

ATP assay

The ATP content was assessed using an ATP Assay Kit (Beyotime, S0026, China). In accordance with the manufacturer's instructions, fGCs were harvested and lysed with ATP extraction buffer, while the background ATP on the detection plate was removed using the detection working solution. Subsequently, the lysed cell samples were added to the detection plate along with the ATP detection working solution. The relative light units (RLU) values from the detection plate were measured utilizing an enzyme-linked immunosorbent assay (ELISA) microplate reader (PerkinElmer, USA), and the ATP levels were determined based on a standard curve. The ATP content was normalized to the total protein amount.

NAD^+/NADH assay

NAD^+/NADH ratio were determined using the NAD^+/NADH Assay Kit with WST-8 (Beyotime, S0175, China). fGCs were collected and lysed with NAD^+/NADH extraction buffer following the manufacturer's instructions. To measure the total NAD^+ and NADH levels, the alcohol dehydrogenase working solution and color solution were added sequentially to the cell lysate. To specifically detect NADH, the cell lysate was heated to 60 °C for 30 minutes before adding the alcohol dehydrogenase working solution and color solution. After a 30-minute incubation at 37 °C, the absorbance at 450 nm was read using a microplate reader (PerkinElmer, USA). The total NAD and NADH levels were normalized to the total protein amount.

Determination of glycogen, free fatty acids and triglyceride

The Glycogen Content Assay Kit (Solarbio, BC0340, China) was utilized for glycogen quantification. fGCs were suspended in extraction buffer, sonicated, and then heated in

boiling water for 20 minutes. Following centrifugation, the supernatant was combined with the detection buffer and incubated in boiling water again for 10 minutes. The absorbance at 620 nm was measured for calculating the glycogen content. For the determination of free fatty acids, the Free Fatty Acid Content Assay Kit (Boxbio, AKFA008C, China) was employed. fGCs were suspended in extraction buffer, sonicated, and subjected to centrifugation. The supernatant was extracted and then underwent sequential coloration. Subsequently, the absorbance at 550 nm was measured for quantifying the content. Triglyceride levels were assessed using the Triglyceride (TG) Test Kit (Njjcbio, A110-1-1, China). fGCs were lysed with RIPA lysis buffer, sonicated, and centrifuged. The resulting supernatant was mixed with the working solution and incubated at 37 °C for 10 minutes. The absorbance at 510 nm was measured to determine the triglyceride content. The measured contents of free fatty acids, glycogen, and triglycerides were normalized to the total protein amount.

PAS Staining

PAS staining was conducted according to the instructions provided with the Periodic Acid-Schiff Staining Kit (Beyotime, C0142S, China). In brief, ovarian tissue samples underwent fixation in a 30% sucrose solution for 48 hours and were subsequently embedded in Optimal Cutting Temperature (OCT) compound (Sakura, 4583, Japan). Notably, cultured follicles were embedded directly in OCT without requiring dehydration. Subsequently, 6 μm-thick sections were obtained using a freezing microtome (Leica, Germany). The sections were washed in phosphate-buffered saline (PBS), fixed in polyformaldehyde at room temperature for 30 minutes, and then rinsed three times in PBS for 5 minutes each. Following this, the sections were treated with Periodic Acid solution for 10 minutes, washed in PBS for 5 minutes, stained with Schiff's reagent for 30 minutes, and again rinsed in PBS for 5 minutes. Finally, the sections were mounted with glycerin gel and examined under a microscope (Olympus, Japan).

Progesterone determination

Serum and culture medium samples were obtained by centrifugation at 4000 rpm for

10 minutes. Ovarian samples were homogenized and centrifuged at 12000 rpm for 10 minutes. The resulting supernatants were aspirated and stored at -20 °C. The Progesterone Radioimmunoassay Kit was procured from Beijing North Institute of Biological Technology (Beijing, China) and the detection was performed by the same institute. Progesterone levels in the ovaries were normalized to the ovarian weight.

Inhibitor and activator treatment protocols

All chemicals utilized in this study were sourced from MCE. The dilution methods and dosages for the pharmaceutical agents were adhered to as per the manufacturers' instructions. To inhibit glycogen breakdown during the glycogen consumption phase in fGCs, GPI-Ingliforib (MCE, HY-19396, USA), a glycogen phosphorylase inhibitor, was administered intraperitoneally at a dose of 15 mg/kg, 9 hours post hCG injection. For in vitro experiments, 40 nM insulin (MCE, HY-P0035, USA) was supplemented into the ovulation/luteinization medium to activate the insulin signaling pathway in fGCs. Concurrently, 100 nM BMS-536924 (MCE, HY-10262, USA) was employed to suppress insulin signaling. Furthermore, 10 μM C16-PAF (MCE, HY-108635, USA) and 40 μM U0126 (MCE, HY-12031A, USA) were incorporated into the ovulation/luteinization medium to activate and inhibit the Ras/Raf/Mek/Erk signaling cascade, respectively.

Electrophoretic mobility shift assay (EMSA)

The RUNX1 Coding sequence was cloned into the pcDNA3.1-3XFlag plasmid (Addgene, China) for overexpression. Flag-tagged RUNX1 proteins were immunoprecipitated using an anti-Flag antibody (Beyotime, P2271, China). The elution of proteins from the antibody was carried out with elution buffer (0.1 M glycine, pH 2.7) and then neutralized using a neutralization buffer (1 M Tris, pH 8.5). Biotin-labeled DNA probes obtained from Genecreate (China) were utilized for the DNA EMSA, conducted with the Chemiluminescent EMSA Kit (Beyotime, GS009, China), following the manufacturer's instructions. In brief, recombinant Flag-RUNX1 and biotin-labeled DNA probes were incubated in binding buffer for 30 minutes at room temperature before being separated on a 4% native polyacrylamide gel at 100 V in TBE buffer (Beyotime, R0223, China). Subsequently, the DNA-protein complexes were

transferred onto Amersham Hybond-N^+ membranes (Cytiva, RPN1510B, USA), blotted with HRP-conjugated streptavidin, and visualized via autoradiography.

ChIP-qPCR

fGCs samples were fixed in 10 mL of DMEM/F-12 (Gibco, 11320033, USA) supplemented with 1% formaldehyde (CST, 12606S, USA) for 10 minutes at room temperature with rotation. The reaction was halted by adding 1 mL of 1.5 M glycine and rotating for an additional 5 minutes at room temperature. Subsequently, the samples were transferred to a 1.5 mL centrifuge tube (Axygen, MCT-150-C, USA) containing PBS for washing. The cell pellets were then lysed in cytomembrane lysis buffer at 4°C for 15 minutes with agitation every 5 minutes. This buffer contained 10 mM HEPES (pH 7.9), 0.5% IGEPAL-CA630, 1.5 mM MgCl2, 10 mM KCl, and a protease inhibitor cocktail. Following cytoplasmic lysis, nuclear lysis was carried out using a buffer containing 1% SDS, 10 mM EDTA, 50 mM Tris (pH 8.1), and a protease inhibitor cocktail, for an additional 15 minutes at 4°C. The sonication of chromatin was performed using an ultrasonic disintegrator (Bioruptor Plus, Belgium) to fragment DNA into sizes ranging from 200 to 500 bp. The sonicated samples were then centrifuged at 12,000 g for 2 minutes. The supernatant was diluted in ChIP IP buffer, which contained 0.01% SDS, 1% Triton X-100, 2 mM EDTA, 50 mM Tris-HCl (pH 8.0), 150 mM NaCl, and a protease inhibitor cocktail. Immunoprecipitation was carried out using 5 μg of anti-RUNX1 antibody (25315-1-AP, Proteintech, USA) and the corresponding control IgG added to protein A/G Dynabeads (Abclonal, RM02915, China), followed by an overnight incubation at 4°C. The beads were washed, eluted, and reverse cross-linked. DNA purification was performed using the AFTSpin Multifunction DNA Purification Kit (Abclonal, RK30100, China). Subsequently, the DNA was utilized for qPCR analysis with specific primers. The primer sequences are detailed in Table S1.

Luciferase reporter assay

To construct the reporter vectors, the promoter regions of *Insr* and *Igf1r* were amplified and inserted into the PGL3-Basic luciferase reporter vector (Promega, USA) using the ClonExpress Ultra One Step Cloning Kit (Vazyme, C115-01, China). Simultaneously, the promoter regions of *Insr* and *Igf1r* containing single base mutations were inserted

into the PGL3-Basic luciferase reporter vector using the Mut Express II Fast Mutagenesis Kit (Vazyme, C214-01, China). HEK293T cells were seeded in a 24-well plate and incubated for 24 hours. Subsequently, the RUNX1 overexpression vector, the constructed pGL3-Basic reporter vectors, and the pRL-TK vector (Promega, USA) were co-transfected into the cells using the jetPRIME® transfection reagent (Polyplus-transfection, 101000046, France) at a ratio of 96: 96: 1. Following 24 hours of transfection, the cells were lysed in a lysis buffer (100 μL) and subjected to a promoter activity assay using the dual-luciferase reporter assay system (Promega, E1910, USA). The luciferase enzymatic activity was measured with a PE Enspire Multilabel Reader (PerkinElmer, USA). The primers utilized in this experiment are provided in Table S1.

Embryo transfer

Donor mice were superovulated and mated with male mice. Concurrently, estrous mice were chosen as recipients and paired with vasectomized males. The appearance of the vaginal plug marked the initiation of gestation. Donor mice were euthanized on the third day of gestation, and the blastocysts were flushed and placed in KSOM medium (Sigma, MR-101, USA). 6 blastocysts were transferred to each side of the recipient's uterine horn, and the deliveries were recorded.

Statistics analysis

Statistical analyses were using GraphPad Prism 10.0 (GraphPad). Data were expressed as the mean ± SD. Two-tailed unpaired Student's t test and one-way analysis of variance followed by Tukey's post hoc test were used to analyze the statistical significance between two groups and among multiple groups, respectively. Chi-squared test was used in the comparison between the percentages. The statistical significance was set at P-value < 0.05.

DATA AVAILABILITY

All data are available from the corresponding author upon reasonable request.

FUNDING

This research was supported by the Biological Breeding-Major Projects in National Science and Technology, Grant/Award Number: 2023ZD04049;

Fundamental Research Funds for the Central Universities (2662023DKPY001) and the National Natural Science Foundation of China (31701301).

SUPPORTING INFORMATION

This article contains supporting information.

ACKNOWLEDGEMENTS

We extend our deepest appreciation and respect to Mrs. Fu Bijun, Dr. He's mother, for her genuine care and encouragement throughout this project.

AUTHORS' CONTRIBUTION

C.H. conceived, designed, performed, funded the experiments, analysis the data, and wrote the manuscript; J.L., Q.L., C.L., G.L., and X.L. anticipated in experiment design and conduction, data analysis, and manuscript preparation; X.W., Y.W., R.L., H.W., H.S., W.K., Z.R., Z.W., B.T., C.W., X.J., and Q.W. assisted with sample collection and experiments conduction; C.H., J.L., Q.L., C.L., G.L., and X.L. revised this manuscript. H.C., G.L., and Q.X. supervised this project. All authors approved the final version.

DECLARATION OF INTERESTS

The authors declare that they have no conflicts of interest with the contents of this article.

REFERENCES

1. JoAnne, S.R., L. Zhilin, and S. Masayuki, *Chapter 22 - Ovulation.* 2015: p. 997-1021.
2. Robker, R.L., J.D. Hennebold, and D.L. Russell, *Coordination of Ovulation and Oocyte Maturation: A Good Egg at the Right Time.* Endocrinology, 2018. **159**(9): p. 3209-3218.
3. Baerwald, A.R., G.P. Adams, and R.A. Pierson, *Characterization of ovarian follicular wave dynamics in women.* Biol Reprod, 2003. **69**(3): p. 1023-31.
4. Stocco, C., C. Telleria, and G. Gibori, *The molecular control of corpus luteum formation, function, and regression.* Endocr Rev, 2007. **28**(1): p. 117-49.
5. Jabbour, H.N., et al., *Endocrine regulation of menstruation.* Endocr Rev, 2006. **27**(1): p. 17-46.

6. Wang, X., S.P. Wu, and F.J. DeMayo, *Hormone dependent uterine epithelial-stromal communication for pregnancy support.* Placenta, 2017. **60 Suppl 1**(Suppl 1): p. S20-s26.
7. Kathryn, J.W. and S.R. Robert, *Luteal angiogenesis and its control.* Theriogenology, 2016. **86**(1): p. 221-228.
8. Lu, E., et al., *Inflammation and angiogenesis in the corpus luteum.* J Obstet Gynaecol Res, 2019. **45**(10): p. 1967-1974.
9. Xu, X., et al., *Imaging and tracing the pattern of adult ovarian angiogenesis implies a strategy against female reproductive aging.* Sci Adv, 2022. **8**(2): p. eabi8683.
10. Taim, B.C., et al., *The Prevalence of Menstrual Cycle Disorders and Menstrual Cycle-Related Symptoms in Female Athletes: A Systematic Literature Review.* Sports Med, 2023. **53**(10): p. 1963-1984.
11. *Diagnosis and treatment of luteal phase deficiency: a committee opinion.* Fertility and Sterility, 2021. **115**(6): p. 1416-1423.
12. Duncan, W.C., *The inadequate corpus luteum.* Reprod Fertil, 2021. **2**(1): p. C1-c7.
13. Shi, L., et al., *Hotspots and frontiers in luteal phase defect research: An in-depth global trend bibliometric and visualization analysis over a 52-year period.* Heliyon, 2024. **10**(15): p. e35088.
14. JoAnne, S.R. and A. Mario, *Endocrine, Paracrine, and Autocrine Signaling Pathways That Regulate Ovulation.* Trends in Endocrinology & Metabolism, 2018. **29**(5): p. 313-325.
15. Khoo, K.H., C.S. Verma, and D.P. Lane, *Drugging the p53 pathway: understanding the route to clinical efficacy.* Nature Reviews Drug Discovery, 2014. **13**(3): p. 217-236.
16. Haraguchi, H., et al., *Mdm2-p53-SF1 pathway in ovarian granulosa cells directs ovulation and fertilization by conditioning oocyte quality.* Faseb j, 2019. **33**(2): p. 2610-2620.
17. Wang, X., et al., *Granulosa Cell-Layer Stiffening Prevents Escape of Mural Granulosa Cells from the Post-Ovulatory Follicle.* Advanced Science, 2024. **11**.
18. Devoto, L., et al., *The human corpus luteum: life cycle and function in natural cycles.* Fertil Steril, 2009. **92**(3): p. 1067-1079.
19. Grøndahl, M.L., et al., *Specific genes are selectively expressed between cumulus and granulosa cells from individual human pre-ovulatory follicles.* Mol Hum Reprod, 2012. **18**(12): p. 572-84.
20. Rolaki, A., et al., *Luteogenic hormones act through a vascular endothelial growth factor-dependent mechanism to up-regulate alpha 5 beta 1 and alpha v beta 3 integrins, promoting the migration and survival of human luteinized granulosa cells.* Am J Pathol, 2007. **170**(5): p. 1561-72.
21. Franz, M.B., et al., *Small GTPases are involved in sprout formation in human granulosa lutein cells.* Arch Gynecol Obstet, 2013. **287**(4): p. 819-24.
22. Fraser, H.M. and W.C. Duncan, *Vascular morphogenesis in the primate ovary.* Angiogenesis, 2005. **8**(2): p. 101-16.
23. Johnson, G.P. and K.C. Jonas, *Mechanistic insight into how gonadotropin hormone receptor complexes direct signaling†.* Biol Reprod, 2020. **102**(4): p. 773-783.

24. Yamashita, Y., et al., *Protein kinase C (PKC) increases TACE/ADAM17 enzyme activity in porcine ovarian somatic cells, which is essential for granulosa cell luteinization and oocyte maturation.* Endocrinology, 2014. **155**(3): p. 1080-90.
25. Gonzalez-Robayna, I.J., et al., *Follicle-Stimulating hormone (FSH) stimulates phosphorylation and activation of protein kinase B (PKB/Akt) and serum and glucocorticoid-lnduced kinase (Sgk): evidence for A kinase-independent signaling by FSH in granulosa cells.* Mol Endocrinol, 2000. **14**(8): p. 1283-300.
26. Zhao, Y. and A.A. Adjei, *The clinical development of MEK inhibitors.* Nat Rev Clin Oncol, 2014. **11**(7): p. 385-400.
27. Ben-Jonathan, N., C.R. LaPensee, and E.W. LaPensee, *What can we learn from rodents about prolactin in humans?* Endocr Rev, 2008. **29**(1): p. 1-41.
28. Fan, H.Y., et al., *CCAAT/enhancer-binding proteins (C/EBP)-α and -β are essential for ovulation, luteinization, and the expression of key target genes.* Mol Endocrinol, 2011. **25**(2): p. 253-68.
29. Espey, L.L., et al., *Induction of early growth response protein-1 gene expression in the rat ovary in response to an ovulatory dose of human chorionic gonadotropin.* Endocrinology, 2000. **141**(7): p. 2385-91.
30. Carlos, O.S., et al., *Prostaglandin F2α-induced Expression of 20α-Hydroxysteroid Dehydrogenase Involves the Transcription Factor NUR77*.* Journal of Biological Chemistry, 2000. **275**(47): p. 37202-37211.
31. Blind, R.D., et al., *The signaling phospholipid PIP3 creates a new interaction surface on the nuclear receptor SF-1.* Proc Natl Acad Sci U S A, 2014. **111**(42): p. 15054-9.
32. Dinh, D.T., et al., *Progesterone receptor mediates ovulatory transcription through RUNX transcription factor interactions and chromatin remodelling.* Nucleic Acids Res, 2023. **51**(12): p. 5981-5996.
33. Rieusset, J., *The role of endoplasmic reticulum-mitochondria contact sites in the control of glucose homeostasis: an update.* Cell Death Dis, 2018. **9**(3): p. 388.
34. Aoyama-Ishiwatari, S. and Y. Hirabayashi, *Endoplasmic Reticulum-Mitochondria Contact Sites-Emerging Intracellular Signaling Hubs.* Front Cell Dev Biol, 2021. **9**: p. 653828.
35. Plewes, M.R., et al., *Luteal Lipid Droplets: A Novel Platform for Steroid Synthesis.* Endocrinology, 2023. **164**(9).
36. Wu, G., et al., *Lactylation drives hCG-triggered luteinization in hypoxic granulosa cells.* Int J Biol Macromol, 2024. **280**(Pt 4): p. 135580.
37. Cooke, I.D., *The corpus luteum.* Hum Reprod, 1988. **3**(2): p. 153-6.
38. Augustin, H.G., *Vascular morphogenesis in the ovary.* Baillieres Best Pract Res Clin Obstet Gynaecol, 2000. **14**(6): p. 867-82.
39. Gougeon, A., *Regulation of ovarian follicular development in primates: facts and hypotheses.* Endocr Rev, 1996. **17**(2): p. 121-55.
40. Ozturk, S., *Molecular determinants of the meiotic arrests in mammalian oocytes at different stages of maturation.* Cell Cycle, 2022. **21**(6): p. 547-571.
41. Wen, J., et al., *Effects of glucose metabolism pathways on nuclear and cytoplasmic maturation of pig oocytes.* Scientific Reports, 2020. **10**(1): p. 2782.

42. Simerman, A.A., et al., *Intrafollicular cortisol levels inversely correlate with cumulus cell lipid content as a possible energy source during oocyte meiotic resumption in women undergoing ovarian stimulation for in vitro fertilization.* Fertil Steril, 2015. **103**(1): p. 249-57.
43. Nandi, S., et al., *Follicular fluid concentrations of glucose, lactate and pyruvate in buffalo and sheep, and their effects on cultured oocytes, granulosa and cumulus cells.* Theriogenology, 2008. **69**(2): p. 186-196.
44. Chahal, N., et al., *Direct impact of gonadotropins on glucose uptake and storage in preovulatory granulosa cells: Implications in the pathogenesis of polycystic ovary syndrome.* Metabolism, 2021. **115**: p. 154458.
45. Bechmann, L.P., et al., *The interaction of hepatic lipid and glucose metabolism in liver diseases.* J Hepatol, 2012. **56**(4): p. 952-64.
46. Nielsen, J., et al., *Human skeletal muscle glycogen utilization in exhaustive exercise: role of subcellular localization and fibre type.* J Physiol, 2011. **589**(Pt 11): p. 2871-85.
47. Chen, J., et al., *Hepatic glycogenesis antagonizes lipogenesis by blocking S1P via UDPG.* Science, 2024. **383**(6684): p. eadi3332.
48. Chilvers, R.A., et al., *Development of a novel protocol for isolation and purification of human granulosa cells.* J Assist Reprod Genet, 2012. **29**(6): p. 547-56.
49. Blondel, V.D., et al., *Fast unfolding of communities in large networks.* Journal of Statistical Mechanics: Theory and Experiment, 2008. **2008**: p. P10008.
50. Mantri, M., et al., *A spatiotemporal molecular atlas of the ovulating mouse ovary.* Proceedings of the National Academy of Sciences, 2024. **121**(5): p. e2317418121.
51. Biancalani, T., et al., *Deep learning and alignment of spatially resolved single-cell transcriptomes with Tangram.* Nature Methods, 2021. **18**(11): p. 1352-1362.
52. Livak, K.J. and T.D. Schmittgen, *Analysis of relative gene expression data using real-time quantitative PCR and the 2(-Delta Delta C(T)) Method.* Methods, 2001. **25**(4): p. 402-8.
53. Wang, X., et al., *The FSH-mTOR-CNP signaling axis initiates follicular antrum formation by regulating tight junction, ion pumps, and aquaporins.* J Biol Chem, 2023. **299**(8): p. 105015.